Macromolecular Materials and Engineering

Macromolecular Materials and Engineering Open Access

www.mame-journal.de

RESEARCH ARTICLE OPEN ACCESS

Polyamide12-Meta-Composites with Excellent Mechanical Performance, Shape-Memory, Flame Retardancy and 3D/4D Printability

Kaveh Rahmani[1] | Keun Park[2] | Mahdi Bodaghi[1]

[1]Department of Engineering, School of Science and Technology, Nottingham Trent University, Nottingham, UK | [2]Department of Mechanical Design and Robot Engineering, Seoul National University of Science and Technology, Seoul, Republic of Korea

Correspondence: Mahdi Bodaghi (mahdi.bodaghi@ntu.ac.uk)

Received: 21 January 2026 | **Revised:** 11 March 2026 | **Accepted:** 18 March 2026

Keywords: CNT-bamboo charcoal | flammability | metamaterials | polyamide 12 | shape-memory | 3D/4D printing

ABSTRACT

Achieving multifunctional polymer composites that combine mechanical strength, thermal stability, flame retardancy, and shape-memory capability while remaining compatible with additive manufacturing remains challenging. In this work, a comprehensive materials library of fused filament fabrication (FFF)-printable polyamide 12 (PA12) composites was developed using bamboo charcoal (BC), a BC/carbon nanotube (BC/CNT) hybrid, and conventional glass fiber (GF) and carbon fibers (CF). PA12/BC and PA12/BC/CNT composites were compounded, extruded into filaments, and systematically characterized in terms of microstructure, wettability, thermomechanical behavior, flammability, shape-memory performance, and mechanical properties at ambient and elevated temperatures. The BC/CNT hybrid represents the key innovation of this study, enabling a synergistic reinforcement strategy that simultaneously enhances stiffness, strength, damping, thermal stability, flame retardancy, and hydrophobicity while preserving excellent shape-memory behavior. In contrast, GF and CF reinforced composites provide higher stiffness and strength but suppress shape-memory functionality. Extending beyond material development, architected shape-memory polymer meta-composites with honeycomb, honeycomb-circle hybrid, and auxetic geometries were fabricated via 4D printing. They demonstrated shape-recovery, force-regulating behavior and high energy absorption/dissipation under compression. These results establish BC/CNT-reinforced PA12 as a more sustainable and multifunctional alternative to conventional fibre-reinforced systems for advanced additive manufacturing applications.

1 | Introduction

Additive manufacturing (AM) has transformed polymer fabrication by enabling geometric freedom, rapid prototyping, and reduced material waste. Among AM methods, fused filament fabrication (FFF) is widely used because it is inexpensive, straightforward to implement, and compatible with many thermoplastic feedstocks [1, 2]. These capabilities have supported the expansion of polymer composites and, more recently, the development of 3D/4D printing concepts that couple material formulations with printed architectures to achieve enhanced functional performance [3, 4]. As a result, FFF is increasingly adopted for manufacturing high-performance thermoplastic composites in a practical manner [5, 6].

Engineering thermoplastics such as polyamides (nylons) are widely used in automotive, sports equipment, robotics, and general engineering due to their favorable mechanical and thermal properties [7, 8]. Compared with degradable polymers such as PLA, Polyamide 12 (PA12) is non-degradable and maintains stable

performance over a wide temperature range. PA12 is therefore widely used in the automotive sector, for example in oil-resistant tubing, cables, packaging films, and impact-resistant components such as bumpers [9, 10]. However, PA12 can still be limited under demanding service conditions where high stiffness, impact resistance, thermal stability, and functional responses (e.g., shape-memory behavior) are required simultaneously. Industrial PA12 parts are predominantly produced by injection molding, which is effective for high-volume manufacturing but involves complex tooling and long lead times, limiting on-demand or site-specific production [11, 12]. In contrast, FFF AM is a tool-less, CAD-driven process that enables rapid, low-cost production and fast design iteration. As a result, FFF is increasingly used to fabricate functional components and prototypes for automotive, construction, and sporting applications [13, 14].

The use of short fibers, particulates, and nanomaterials is a well-established strategy for improving thermoplastic performance [15]. Short fibers can enhance stiffness, strength, and dimensional stability, with glass fibers (GF) and carbon fibers (CF) being among the most common reinforcements due to their strong strengthening and stiffening effects [16]. However, fiber additions often increase brittleness and can suppress functional behaviors such as shape-memory capability. Consequently, conventional fiber-reinforced composites may struggle to meet the multifunctional requirements of advanced applications. In this context, incorporating functional fillers such as carbon nanotubes (CNT) into a thermoplastic has been proposed as an alternative approach to enhance mechanical properties. For instance, Rahmani et al. [17] demonstrated that CNT-reinforced composites exhibit improved mechanical properties. Natural reinforcements such as bamboo-derived materials offer a sustainable alternative to conventional fibers. Among them, bamboo charcoal (BC) has attracted growing interest as a multifunctional additive due to its abundance, rapid renewability, good mechanical robustness, and favorable compatibility with polymer matrices [18, 19]. When incorporated into thermoplastics, BC can improve mechanical performance and surface characteristics such as hydrophobicity. In parallel, the demand for flame-retardant materials in automotive, aerospace, transportation, and construction sectors continues to increase. However, many conventional flame retardants, including halogenated and phosphorus-based systems, have been restricted or banned in the European Union since 2021 because of environmental and health concerns, and they often compromise mechanical properties [20, 21]. In this context, BC emerges as a promising bio-based additive that can simultaneously reinforce thermoplastics and contribute to flame resistance without relying on hazardous chemicals [14, 18].

While the individual benefits of BC [19] and CNT [17] have been reported for thermoplastic composites, their individual and combined effects in FFF-printed PA12 systems remain poorly understood. In particular, the influence of BC/CNT hybrid reinforcement on process–microstructure–property relationships in additively manufactured PA12 has not yet been systematically investigated. In hybrid systems, BC may act as a natural carbonizing particulate, serving as a heat sink, barrier-forming agent, and surface-energy modifier, while CNT contribute stiffness, strength, and dimensional stability. Nevertheless, it remains insufficiently understood how these reinforcements, both individually and synergistically, affect processing behavior, interfacial structure, hydrophobicity, and thermomechanical performance of FFF-printed PA12 at operational temperatures. In particular, it is unclear whether such reinforcements can enhance flame retardancy and shape-memory behavior without compromising mechanical integrity. These gaps highlight the need for a systematic and application-oriented mapping of material formulations and printed architectures tailored for FFF, alongside fair comparisons with conventional fiber-reinforced systems.

To address these challenges, a library of nature-derived composite materials was developed based on FFF-printable PA12 reinforced with BC, BC/CNT hybrid systems, and conventional glass and carbon fibers. The study encompasses filament preparation, printing, and comprehensive characterization. Shape-memory performance, microstructure, wettability (water contact angle), thermomechanical behavior, flammability, and key mechanical properties (tensile, flexural, impact, and hardness) were evaluated at room and elevated temperatures. The results demonstrate that BC and CNT act synergistically to enhance hydrophobicity and flame retardancy while simultaneously improving stiffness, strength, shape-memory behavior, and energy dissipation. Furthermore, architected meta-composites were developed, exhibiting constant-force tuning and quasi-zero stiffness (QZS) for efficient energy absorption. The results of this research highlight pathways toward lightweight, multifunctional, and sustainable 3D-printed composite components, and identify key material and microstructural parameters, such as reinforcement dispersion, interfacial bonding, and print-induced anisotropy, that govern final performance. These results aim to guide material selection and structural design for next-generation printed components in automotive, sports, and robotic systems, where a balance between performance, cost, and sustainability is required. Figure 1 summarizes the development workflow from material preparation to representative application domains and illustrates scenarios in which FFF offers distinct advantages for PA12-based components.

2 | Composite Materials, Manufacturing and Testing

2.1 | Compounds and Composite Constituents

In this study, PA12, PA12/15 wt.% carbon fiber, and PA12/15 wt.% glass fiber filaments were supplied by Fiberlogy (Poland). Additionally, PA12 filaments reinforced with particulate fillers, including 3 wt.% BC and 3 wt.% BC/1 wt.% CNT, were prepared and used as feedstock materials for FFF of all samples. PA12 filaments are renowned for their exceptional strength and durability, as well as their outstanding resistance to elevated temperatures, alcohols, and various chemicals, making them highly suitable for mechanical and technical applications.

The BC particles, with an approximate size of 25 μm and derived from natural plant sources, were provided as raw particulate reinforcement material (Takesumi Ltd., Japan). A 3 wt.% loading of BC was incorporated due to its functional benefits, including flame retardancy, moisture regulation, and its potential to improve stiffness and energy dissipation when used as a reinforcement in polymer composites [19, 22]. In addition, commercial CNT of the NC7000 type were purchased

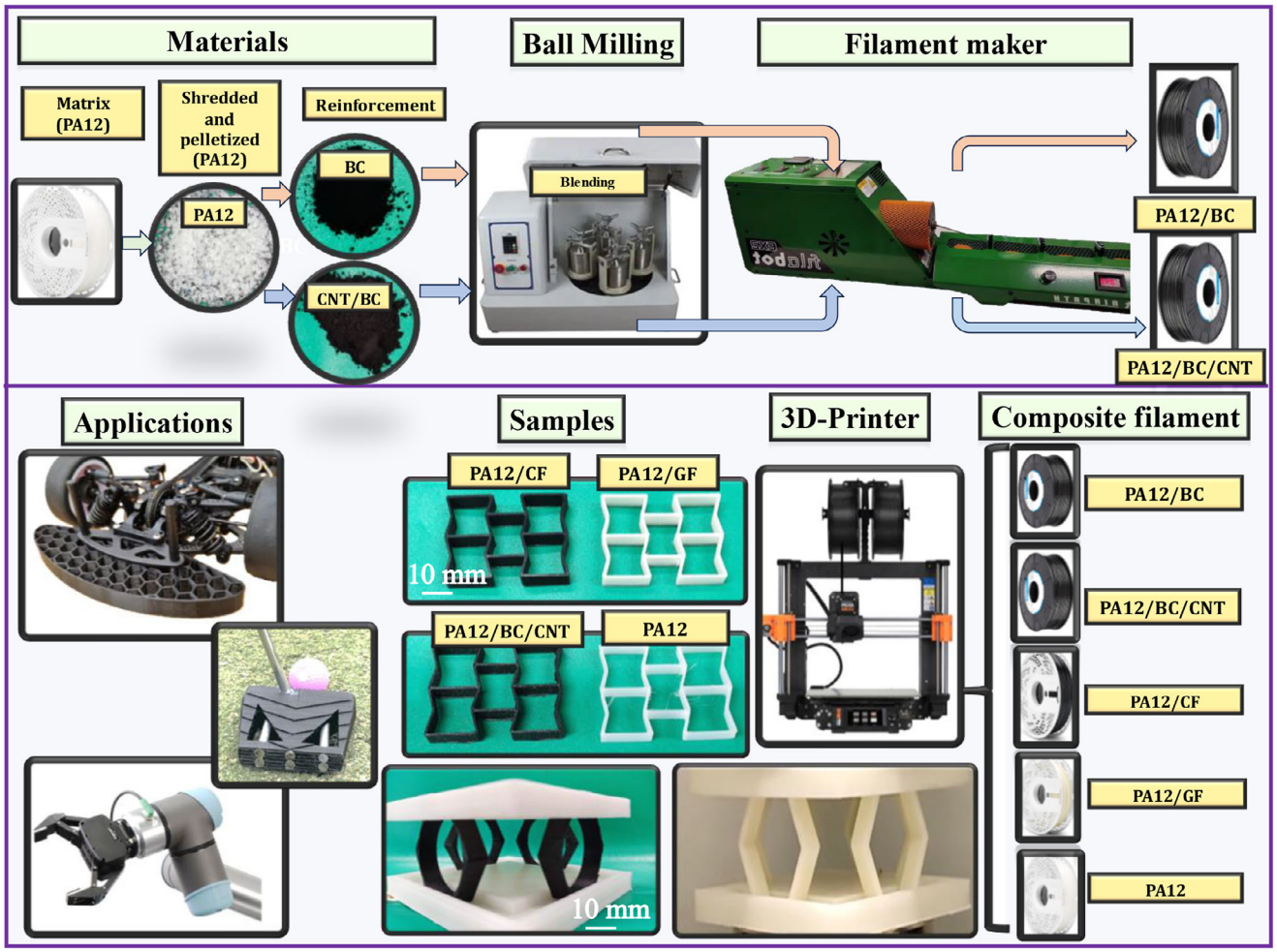

FIGURE 1 | Schematic illustration of the manufacturing workflow for PA12-based composites, from material preparation and filament extrusion to FFF of architected meta-structures. Representative application areas include robotics, sporting, and automotive components.

from Nanocyl S.A. (Sambreville, Belgium). According to the supplier, these CNT exhibit a purity >90%, with an average diameter of 9.5 nm and an average length of 1.5 μm. CNT were added due to their well-established ability to enhance mechanical stiffness. A 1 wt.% loading was selected, as this concentration was reported to provide the most effective improvement [17]. All filaments used in this study had a diameter of 1.75 mm. The investigated materials included PA12 filaments containing 3 wt.% BC, with or without 1 wt.% CNT, as well as PA12/15 wt.% GF and PA12/15 wt.% CF filaments. These are hereafter referred to as PA12/BC, PA12/BC/CNT, PA12/GF, and PA12/CF, respectively.

2.2 | Composite Filament Preparation for FFF 3D Printing

The flowchart in Figure 2 illustrates the process used to produce the PA12 composite filaments. To fabricate PA12/BC and PA12/BC/CNT composite filaments, PA12 filaments were first shredded into small pieces and then pelletised using an extrusion process, and finally, 3 wt.% BC and 3 wt.% BC/1 wt.% CNT were incorporated separately. The resulting mixtures were then dried in a laboratory oven at 80°C for 12 h to eliminate any residual moisture. The production of PA12/BC and PA12/BC/CNT composite filaments consisted of three sequential stages. The first stage involved ball milling the PA12 and BC, as well as the PA12 and BC/CNT composite powder mixtures, at an operating frequency of 30 Hz to ensure uniform dispersion of the reinforcements (Section S2.4). The milling process utilized twelve hard chromium steel balls with a diameter of 10 mm and five steel balls of the same material with a diameter of 15 mm, with a ball-to-powder mass ratio of 1:2 in a 150 mL steel vial. The composites were milled and blended at a rotational speed of 100 rev/min for 10 min to achieve a homogeneous distribution. The second stage was composite extrusion using a Filabot EX2 extruder (USA) equipped with a speed-controlled spooler. The extrusion temperature was maintained between 180°C and 190°C, and the screw speed was set to 30 rpm. This process yielded composite filaments with a consistent diameter of 1.75 ± 0.05 mm. 3) 3D printing using an FFF-based 3D printer (Original Prusa MK4S) under the following printing conditions: nozzle diameter = 0.4 mm, printing speed = 80 mm/s, linear infill pattern, nozzle temperature = 245°*C*, and bed temperature = 90°*C*.

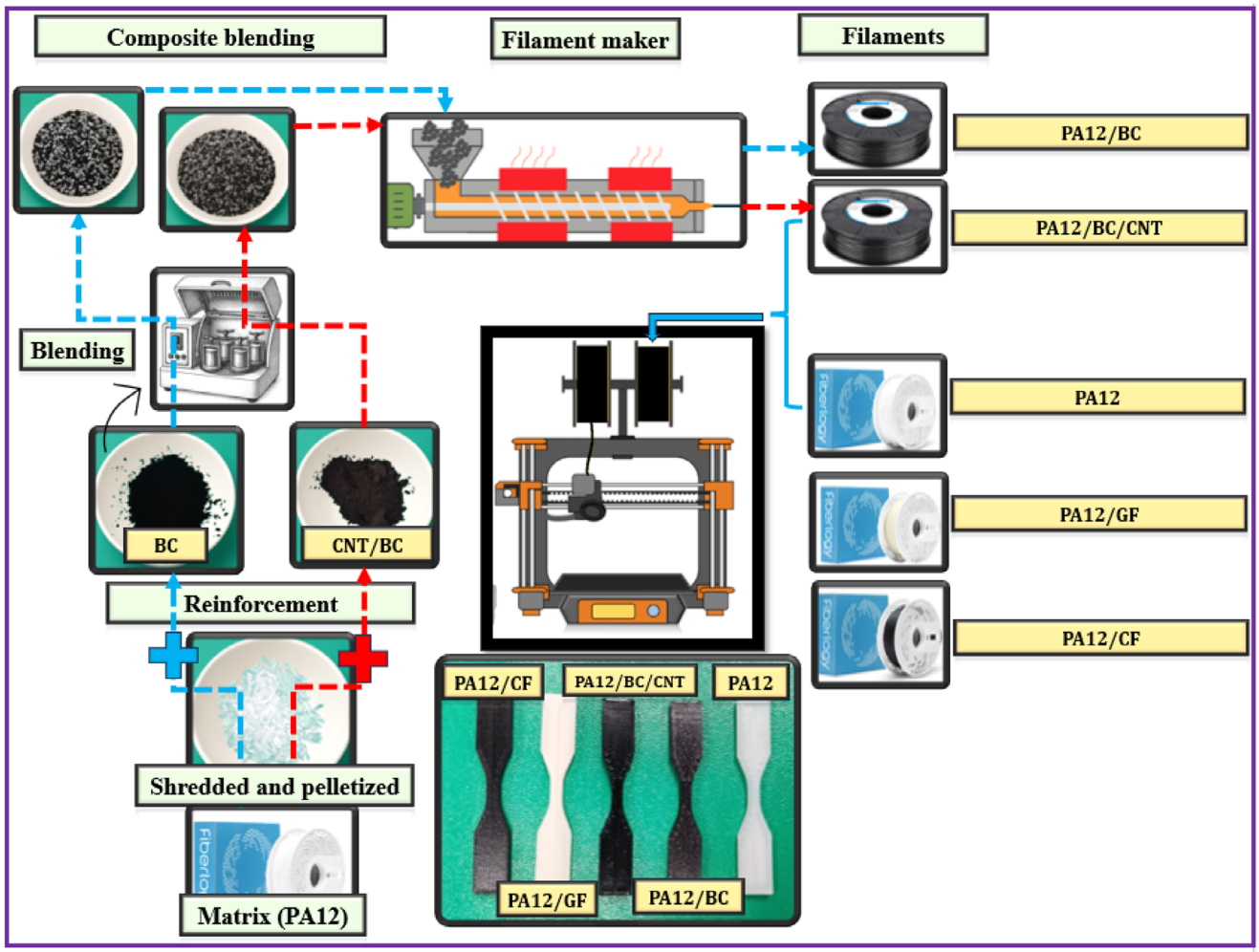

FIGURE 2 | Schematic of the manufacturing workflow for PA12 composites, including blending of pelletized PA12 with BC and CNT particles, filament extrusion, and subsequent 3D printing of test specimens.

3 | Material Characterization

3.1 | Microstructural Analysis

Scanning electron microscopy (SEM) was employed to examine microstructural analysis to assess the BC and CNT distribution and the fracture surfaces to understand the bonding between PA12 and reinforcements. A JSM-7100F LV FEG machine was employed for this purpose. Before imaging, the samples were gold sputter-coated with a 5 nm layer to enhance image clarity.

3.2 | Dynamic Mechanical Thermal Analysis (DMTA)

A DMTA machine (DMA 8000, PerkinElmer) was utilized to investigate the thermo-mechanical behaviors in the 3D-printed specimens, as shown in Figure S1 in the supplementary material. Thermomechanical characterization confirms the critical role of the printing process in programming shape-memory performance [23]. Composites were tested in the bending mode using a cantilever beam. The DMTA testing procedure consisted of a temperature ramp from −100°C to 100°C at a rate of 2°C/min. Storage modulus and tan δ vs temperature were calculated throughout the test procedure.

3.3 | Shape Memory Analysis

The capacity of fabricated composites to return to their original shape under thermal stimulation was evaluated using cold/hot programming (CP/HP) protocols, as displayed in Figure 3a,b. This assessment aimed to investigate the impact of reinforcements GF, CF, BC, and BC/CNT on the shape memory effect (SME) of PA12 matrix 3D-printed composites. The sample has dimensions of 50 mm in length, 1 mm in width, and 1 mm in thickness. The experiments were conducted in triplicate, and average values were reported for each series of tests. The shape-memory behavior observed in the developed PA12-based composites corresponds to a thermally activated one-way shape-memory effect. In this system, temporary shape fixation is achieved through mechanical deformation CP/HP, and recovery to the original geometry occurs only upon reheating above glass transition temperature (T_g). After recovery, the material remains in its original configuration and does not exhibit spontaneous reversible shape change under cyclic thermal loading without reprogramming.

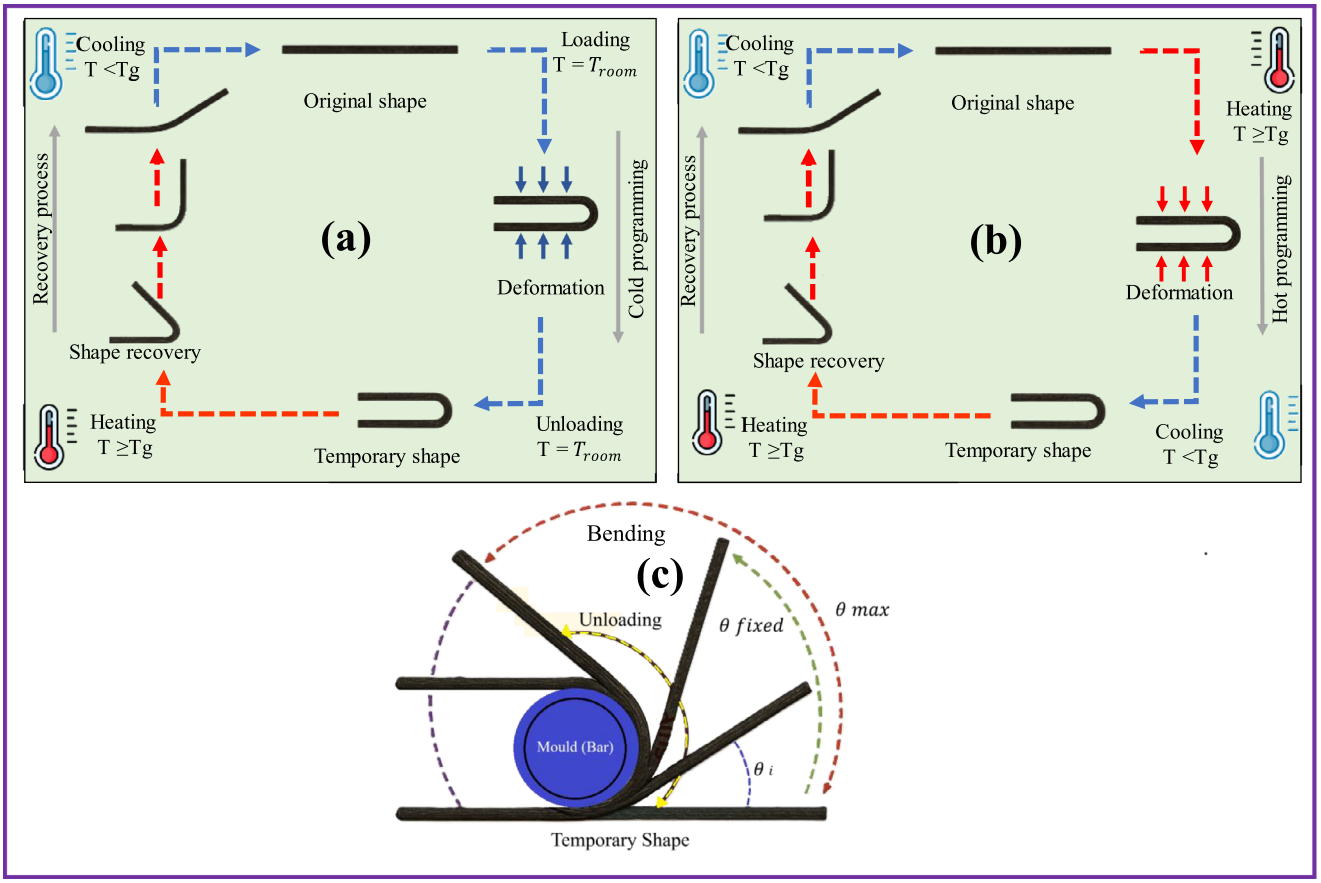

FIGURE 3 | Schematic explanation of the SME test. (a, b) the CP and HP program on the developed composite. (c) bending angle measured at each stage.

In the HP approach, the samples were initially heated to a temperature exceeding the T_g. They were then deformed by applying sufficient force around a bar of 20 mm in diameter, as depicted in Figure 3c. The maximum bending angle achieved, recorded as θ_{max}, was noted during the shape fixation phase (Figure 3c). After applying the external force and deforming the samples, they were cooled to ambient lab temperature (25°C). Once stabilized, the bar and force were removed, and the fixed angle was designated as θ_{fixed}. Subsequently, the samples were gradually reheated to maximise recovery before being cooled again. The final bending angle, θ_i, was carefully documented.

In the CP method, the samples were deformed at ambient lab temperature to achieve θ_{max}. The force was then released to record the fixed angle θ_{fixed}, which resulted from residual inelastic strains in the material. Afterward, a heating-cooling process similar to the HP method was applied. Finally, θ_i was measured to show the extent of partial or full recovery from the inelastic deformations. The samples were heated using hot water set to the $T \geq T_g$ temperature. The shape fixation and recovery ratios were calculated based on the angles recorded as follows [24]:

$$Shape\ fixing\ (S_f) = \frac{\theta_{fixed}}{\theta_{max}} \times 100 \quad (1)$$

$$Shape\ recovery\ (S_r) = \frac{\theta_{max} - \theta_i}{\theta_{max}} \times 100 \quad (2)$$

3.4 | Water Contact Angle Measurement (WCA)Analysis

Surface energy and wettability are critical properties for polymers like polyamides, especially in applications involving frequent fluid contact, such as in the automotive industry. For instance, within engine compartments, these properties provide resistance to moisture and oil, while in interior consoles they prevent moisture-induced degradation, maintaining paint integrity and strong adhesion of coatings. Consequently, they enhance the durability and performance of automotive polymer components. To evaluate these properties in novel PA12 composites, wettability testing was performed with an optical tensiometer (Theta Lite) (Figure S2). A sample was placed on the testing stage, and a 5 µL water droplet was dispensed onto its surface via an injector. A CCD camera recorded the data throughout the process, which was then analyzed using the One Attention software.

3.5 | Flammability Analysis

The flammability properties of the composites were analyzed to evaluate the resistance of composite materials to flame propagation. It matters in different industries, including the automotive sector, for applications such as dashboards, door panels, and center console panels, using an Underwriters' Laboratories (UL-94) method. The flammability was assessed in accordance with

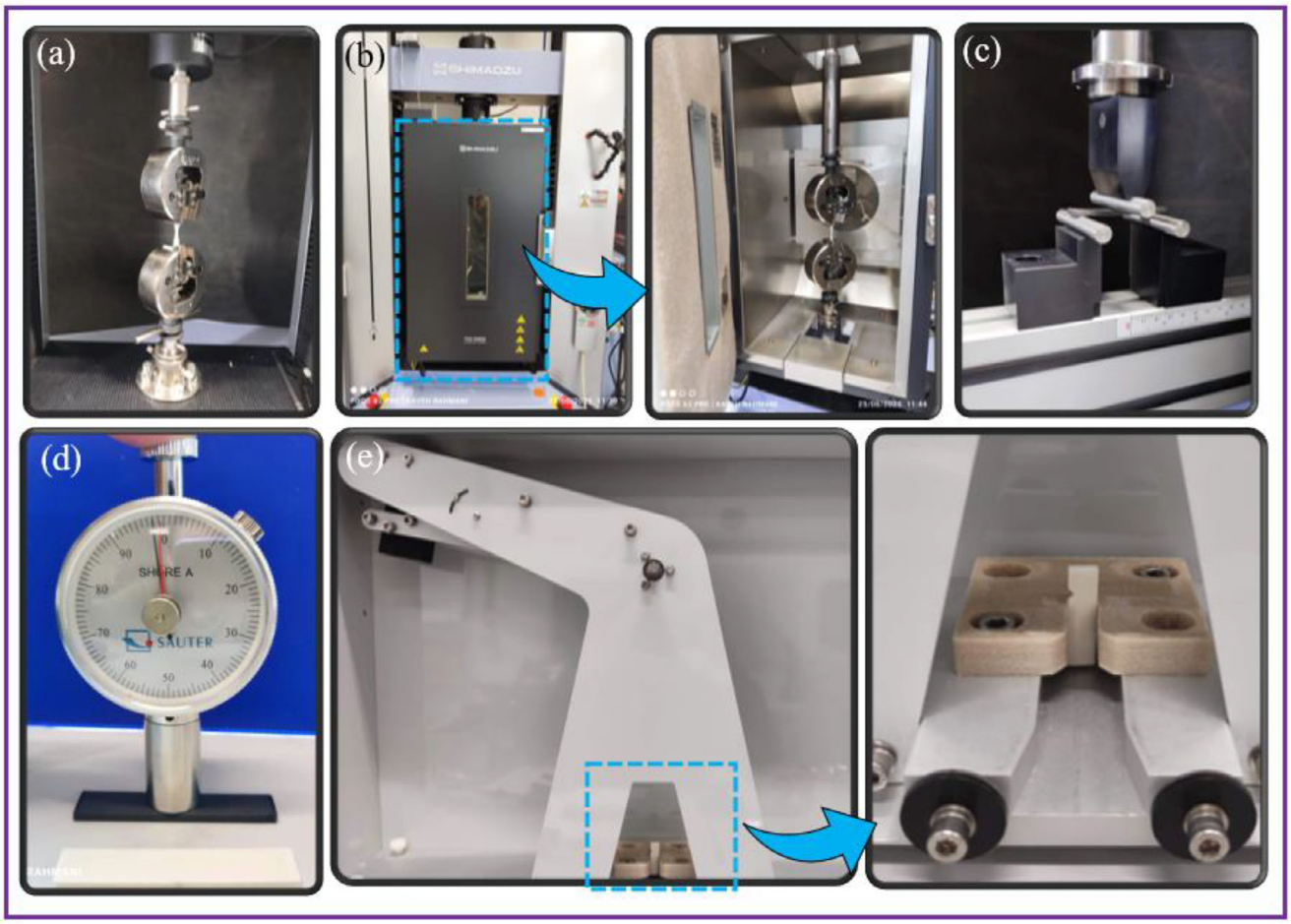

FIGURE 4 | Image of PA12 and PA12 composite under (a) tensile testing, (b) a temperature chamber with a clamping system for tensile testing, (c) flexure testing, (d) a hardness test, (e) impact testing.

ASTM D635-22 to measure the burning rate and duration in a horizontal position. Horizontally mounted 3D-printed samples were placed in a fume hood and marked at 25 and 100 mm from one end (Figure S3).

3.6 | Mechanical Properties

a. Tensile tests were conducted on PA12 composites at different temperatures, according to the ASTM D638-02 standard. All specimens tested were type V specimens. A Shimadzu AG-X plus machine apparatus was utilized for the tensile tests. The elongation speed was set to 5 mm/min (Figure 4a,b).

b. Flexural tests were also conducted in the same apparatus by replacing the tensile grips with a three-point bending module. Flexural tests were conducted according to the ASTM D790-10 standard. 3D printed specimens were dimensioned according to Figure 4c, and the support span was set to 52.0 mm. Flexural loading rate was set to 5 mm/min.

c. The microhardness measurements were conducted according to the ASTM D2240 standard with the 35° truncated-cone indenter. The applied force was set to 150 g, and the indentation time was set to 10 *s*. The hardness of samples was measured using an analogue durometer, Sauter HB model HBA 100-0, manufactured by Sauter GmbH (Figure 4d). Indentations were performed on the polished surfaces of the fabricated specimens.

d. Impact tests were carried out following the ASTM D6110-04 standard. Composites base PA12 were dimensioned according to Figure 4e. An Izod's impact apparatus (Tec Equipment Ltd., UK) was employed in the tests.

In this study, all mechanical tests were carried out on five specimens per group under ambient laboratory conditions, without any prior conditioning, and results are reported as means ± standard deviations. All samples were 3D printed along their longitudinal axis. Also, Figure 5 presents the ASTM-standard photographs of the 3D-printed specimens.

4 | Results and Discussion

4.1 | Shape Memory Effect

The shape memory behavior of PA12 composites (PA12, PA12/BC, PA12/BC/CNT, PA12/GF, PA12/CF) was studied using cold and hot programming methods, with testing done under temperature monitoring. The goal is to understand how different reinforce-

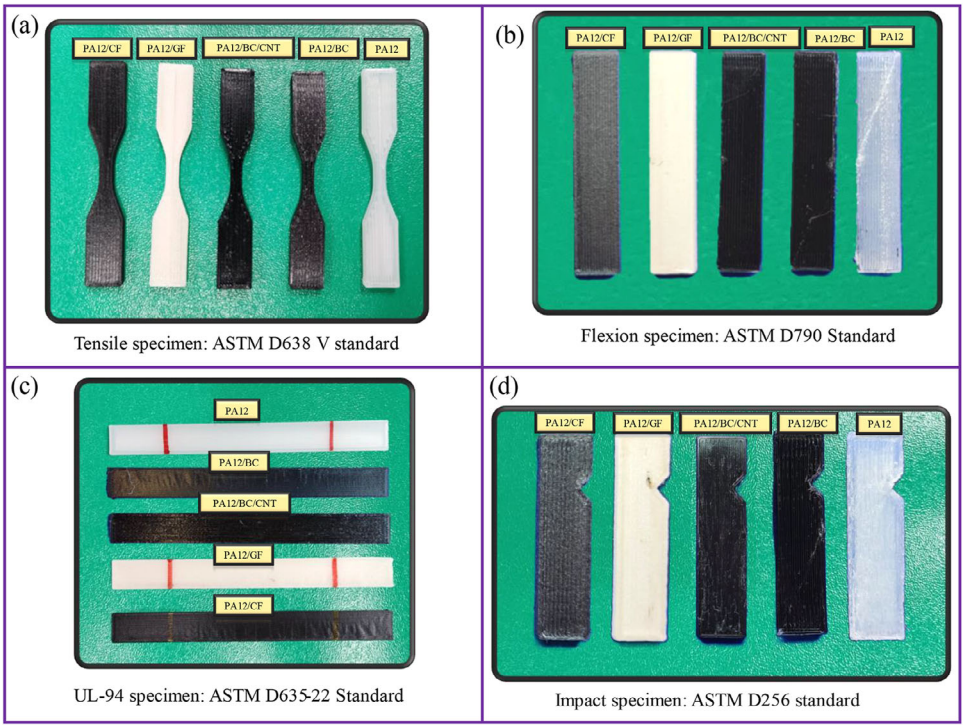

FIGURE 5 | Images of the 3D-printed PA11 composites designed according to ASTM standard, along with the testing method (a) tensile test, (b) flexion test, (c) UL-94, (d) impact test.

ments affect the SME. Figure 6 shows the original, temporarily deformed, and final recovered shapes of the samples after both programming methods. According to Figure 6a, PA12 and composites reinforced with BC and BC/CNT exhibited shape memory properties under both cold and hot programming. These composites showed significant recovery from the deformation caused by loading, which is an important improvement for this class of materials. In contrast, as shown in Figure 6b, the samples reinforced with CF and GF did not show SME when cold-programmed. Even with hot programming, their shape recovery was poor compared to the other samples. This is because the hardness and brittleness of CF and GF, along with potentially weak bonding to the PA12 matrix, hinder shape recovery and can cause separation. Figure 6c highlights shape fixation performance. In hot programming, the ability to hold the temporary shape improved at higher temperatures, with PA12, PA12/BC, and PA12/BC/CNT performing best. Cold programming generally led to poor shape retention due to increased stiffness at room temperature; the CF and GF samples even failed in this mode (Figure 6a). A comparison of shape recovery ratios is presented in Figure 6d.

PA12, PA12/BC, and PA12/BC/CNT achieved the highest recovery over 90% for cold programming and over 95% for hot programming, much higher than the CF and GF reinforced samples. The fixity and recovery ratios were calculated as shown in Figure 6e. Finally, Figure 6f indicates recovery times. PA12 and its BC/CNT composites recovered their shape in 5–6 s, while PA12/GF and PA12/CF were faster, recovering in 3 and 4 s, respectively. This difference is linked to the softer nature of BC and CNT particles. Importantly, adding BC and CNT, especially in cold programming, enhanced the shape recovery capability of the composites, unlike CF and GF reinforcements, which showed no recovery.

It is worth noting that no universally defined minimum threshold exists for shape fixity or recovery ratio to classify a material as a shape-memory polymer. However, the reported values of shape fixity and recovery can vary considerably depending on the material system, deformation mode, and intended application. For instance, Kumar et al. [25] reported a shape fixity ratio of 66.22% as relatively poor, while a recovery ratio of 57.27% was considered weak, whereas higher values of approximately 89% were identified as the best recovery performance within that system. Also, Rahmani et al. [26]. reported relatively low shape fixity values (around 30%–40%) for PLA-based composites.

4.2 | Microstructure Study

The microstructural study was conducted on the surface of the PA12 composites to gain a clearer understanding of the BC and CNT particle distribution and fibers of GF and CF within the PA12 matrix. SEM analysis of the fracture cross-sections reveals distinct morphological changes. The PA12 sample shown in Figure 7a exhibited a smooth, void-free, and homogeneous fracture surface. In contrast, the PA12 composites reinforced with BC and BC/CNT exhibited a uniform particle distribution throughout the matrix, forming clean and strongly bonded interfaces that promote efficient stress transfer and contribute to enhanced stiffness and strength. For the PA12/CF and PA12/GF composites (Figure 7b,c), the glass and carbon fibers were primarily oriented parallel to the fracture surface. These fibers were well integrated into the matrix

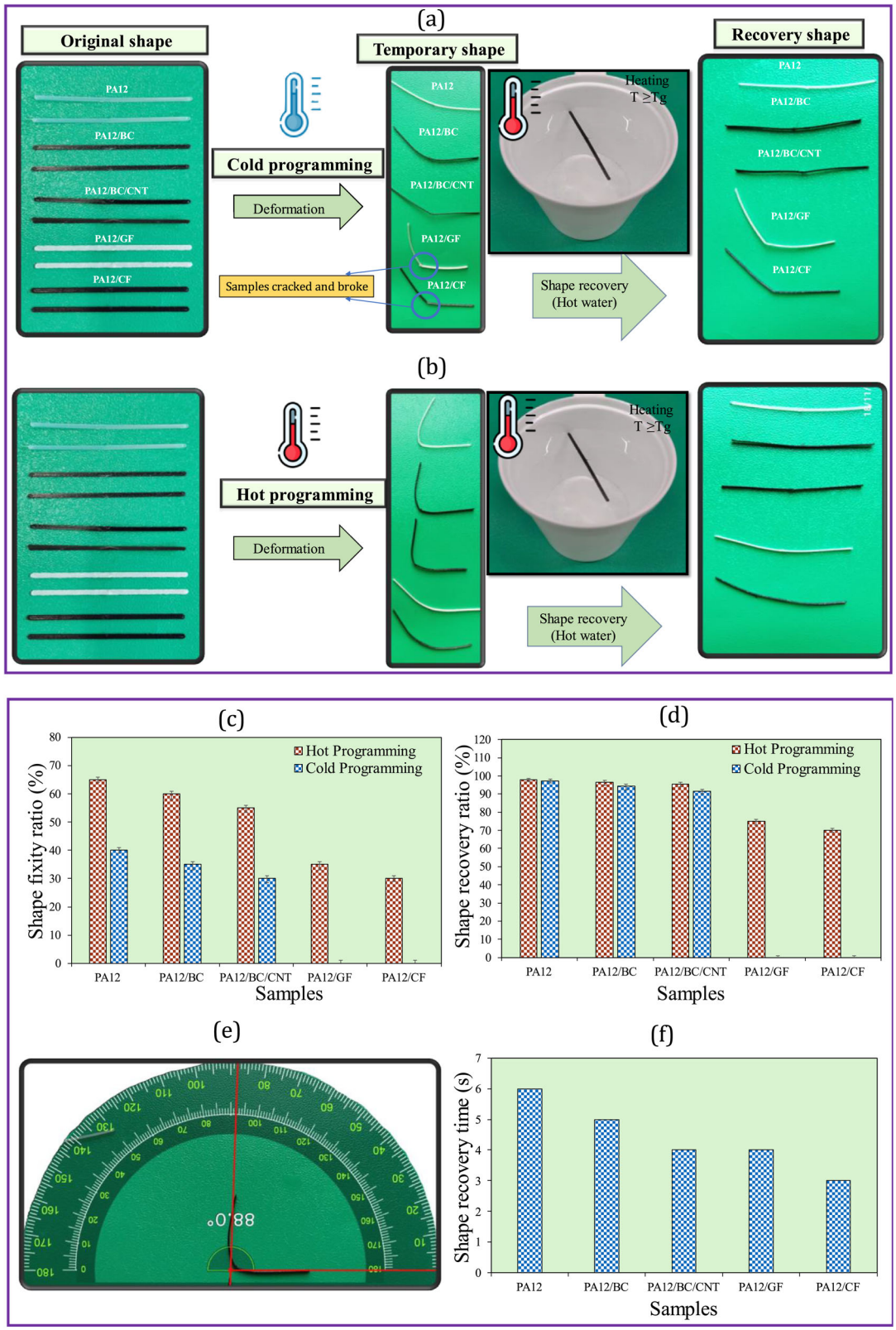

FIGURE 6 | Shape memory test results of original, temporary, and recovered shapes of printed PA12 and PA12 composites. (a) cold-programmed, (b) hot-programmed, illustrated with images at the end of cooling. (c) shape fixity ratio of composites under cold/ hot programming (d) shape recovery ratio of composites under cold/ hot programming (e) measurement of the fixity and recovery ratios (f) shape recovery time of composites under cold/hot programming.

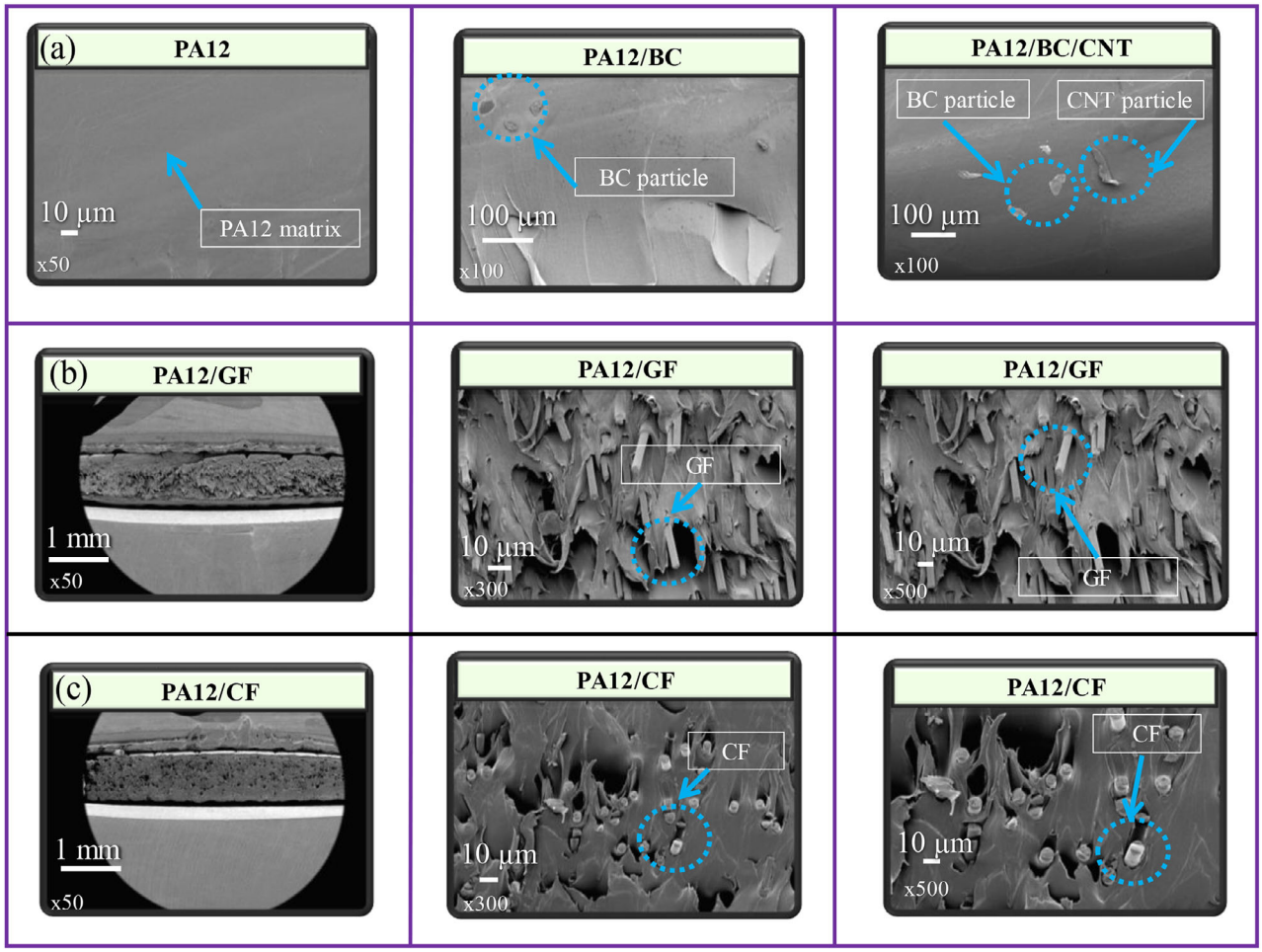

FIGURE 7 | Cross-sectional SEM micrographs at different magnifications of (a) PA12, PA12/BC, and PA12/BC/CNT, (b) PA12/GF, (c) PA12/CF.

and, despite some localized debonding which can act as a barrier to initial crack propagation, served as the primary load-bearing elements, substantially improving the stiffness and strength of the material.

4.3 | Wettability Characteristics

Water contact angle (WCA) testing was used to evaluate the surface wettability of PA12 and its composites. Figure 8a illustrates the evolution of the contact angle from its initial value (A°) to its final stabilized value (B°) over a 10 s period. The results, shown in Figure 8b, reveals a clear trend. PA12 exhibited the lowest and most decreasing angles (from 63.09° to 50.57°), indicating high surface polarity and a tendency for rapid wetting. The incorporation of reinforcements consistently increased hydrophobicity. Composites with BC and BC/CNT showed higher initial angles 70.09° and 76.2°, respectively, which stabilized around 62.4° and 70.3°, suggesting a reduction in surface energy. The PA12/GF composite displayed a similar stable, high angle (from 78.9° to 75.3°). Notably, the PA12/CF composite demonstrated the greatest hydrophobicity, with the highest and most stable contact angles (from 80.95° to 78°). This represents a 34% improvement over PA12 and indicates the strongest resistance to wetting. It is important to note that WCA values of the PA12/BC/CNT achieved competitive values with the glass and carbon fiber composites, potentially due to the high bulk density of CNT. Next, Figure 8b shows that all reinforcements significantly increased the contact angle and suppressed its decay over time. A higher, more stable contact angle signifies lower surface energy, which translates to improved material resistance to fluid absorption, fuel-tank condensation, and environmental degradation.

4.4 | DMTA

Figure 9 illustrates how temperature affects the storage modulus (E′) and tan δ for PA12 and its composites. The T_g, identified from the peak of the tan δ curves in Figure 9a, increases with the addition of reinforcements rising from 49.5°C for PA12 to 58.9°C for the PA12/CF composite (See blue arrow). The data show that the presence of reinforcing materials reduces the tan δ peak, a result of the enhanced storage modulus. As expected, all composites demonstrated higher storage modulus values than PA12, attributable to the stiffening effect of the fibers and the hardness of particles. Figure 9b illustrates that for all materials, the storage modulus experienced a gradual decline as temperature increased to 10°C, due to increased polymer chain mobility. A sharp drop occurred once the temperature surpassed T_g, as the PA12 phase transitioned to a highly mobile state. However, the composite materials maintained significantly higher modulus values above T_g compared to PA12. This is because the hardness and stiffness

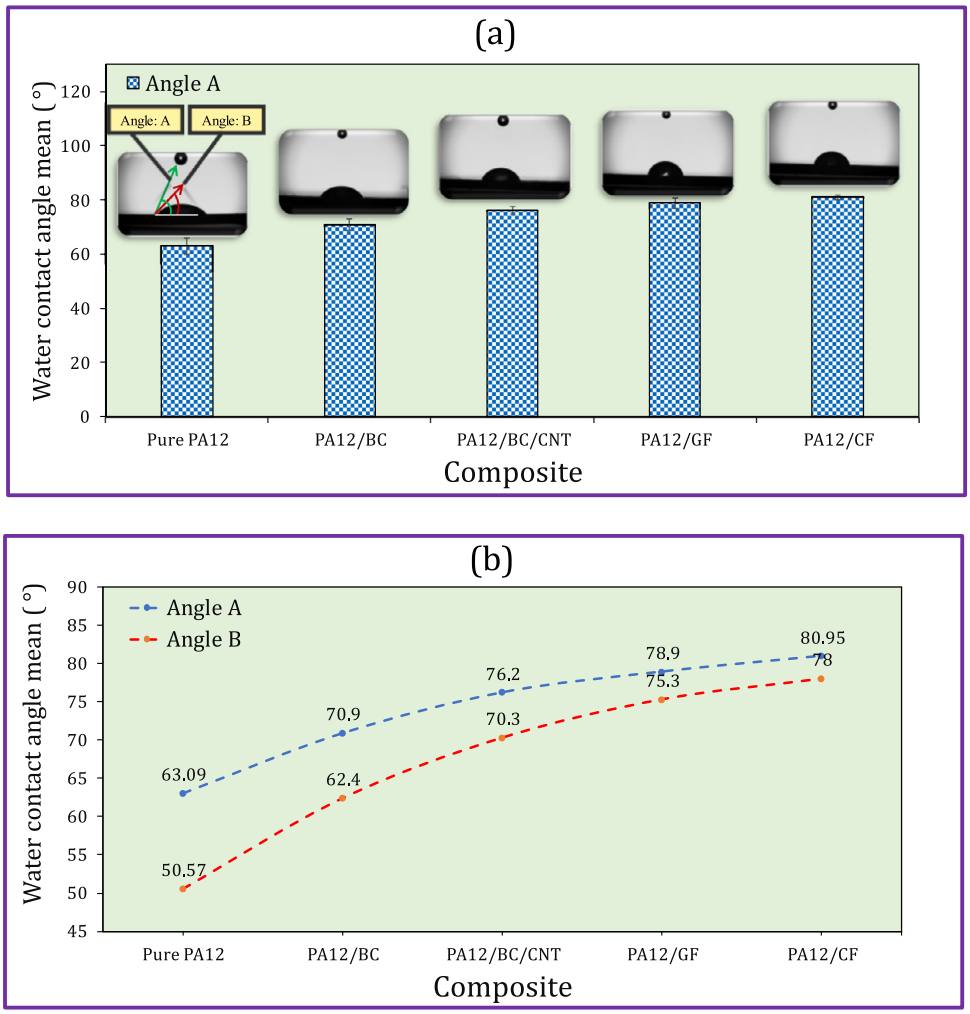

FIGURE 8 | WCA variation for PA12 and PA12 composites, along with (a) images of water droplets after stabilisation, (b) comparison of graphs of the WCA.

of the reinforcements (CNT, BC, GF, and CF) restricted polymer chain mobility and mitigated the modulus reduction. This effect is particularly evident in the PA12/CF composite, which retained a higher storage modulus at elevated temperatures than all other samples. Also displayed result of storage modulusPA12 reinforced with BC/CNT higher from PA12/BC and almost close to the PA12/GF. It should be noted that TGA and DSC analyses could provide additional information on degradation kinetics, T_g, and thermal stability. However, it is out of scope of the current research and could be performed in future endeavor. One may refer to [10] for more details.

4.5 | Flammability Properties

The flammability of the composites was evaluated using the UL-94 horizontal burning test. As shown in Figure 10a, all reinforced samples exhibited significantly lower burning rates than PA12, indicating improved fire retardancy. This enhancement can be attributed to multiple mechanisms, including the formation of insulating char layers promoted by the reinforcements, which act as physical barriers that shield the underlying material from heat and limit the release of flammable volatiles [27]. The most pronounced improvements were observed for the PA12/CF, PA12/GF, and PA12/BC/CNT composites, with burning rate reductions of 40%, 29%, and 25%, respectively, relative to PA12. Notably, the flame-retardant performance of the PA12/BC/CNT composite was comparable to that of the glass- and carbon-fiber-reinforced systems. In addition, the incorporation of BC and CNT effectively suppressed material dripping during combustion, further contributing to reduced flammability. As illustrated in Figure 10b–f, which document the samples before, during, and after testing, these results demonstrate the potential of BC/CNT reinforcements to produce flexible and fire-resistant PA12 composites. Such materials are well suited for meeting fire-safety requirements like those in automotive/construction sector and for example may help mitigate fire-related risks in vehicle applications. It should be noted that PA12 is a non-biodegradable engineering thermoplastic; therefore, the developed composites are not biodegradable under natural environmental conditions. The incorporation of BC, a renewable bio-derived filler, enhances sustainability from a resource-efficiency perspective but does not impart biodegradability to the material system. Nevertheless, unlike thermoset-based composites, PA12-based systems

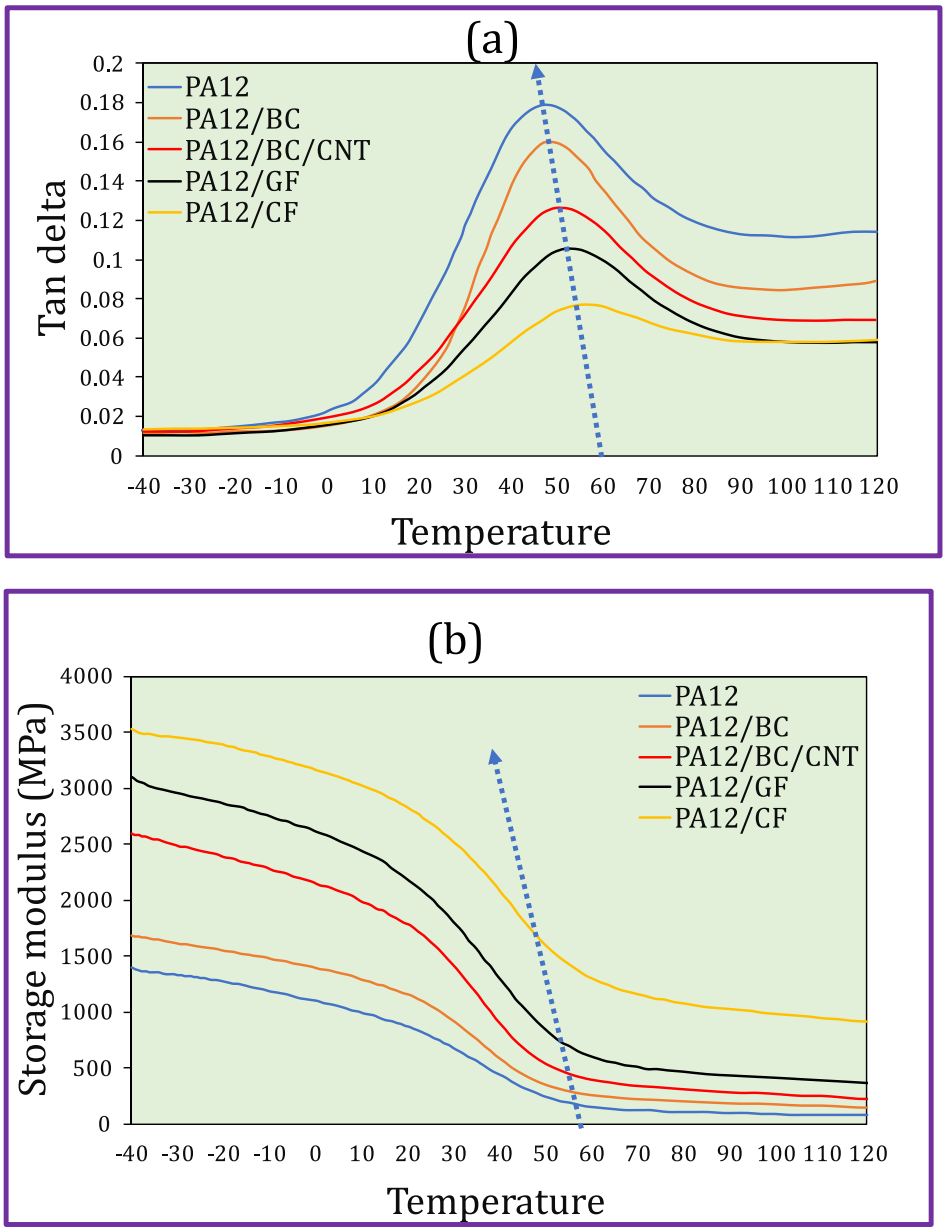

FIGURE 9 | DMTA results of PA12 and PA12 composites, (a) tan δ (b) storage modulus.

retain thermoplastic recyclability potential, which may provide advantages within circular-economy frameworks and controlled end-of-life management strategies.

4.6 | Mechanical Properties

4.6.1 | Tensile Properties

Tensile testing of PA12 and its composites revealed that all additives served as effective reinforcements [28]. The stress-strain curves, the ultimate tensile strength (UTS), and the modulus of elasticity are shown in Figure 11a. The most significant enhancement was observed in the PA12/CF composite, which exhibited a 122% increase in UTS and a 370% increase in modulus compared to PA12. Notably, according to Figure 11b, the composite reinforced with a combination of BC and CNT also performed well, achieving a 67% increase in tensile strength that brought it close to the performance level of the PA12/GF composite (97% increase). Also, Figure 11c illustrates the modulus of PA12/BC/CNT with a high difference from the two samples of PA12 and PA12/BC, and close to the results of the GF and CF reinforced PA12. These mechanical improvements are attributed to two primary mechanisms: 1) The high stiffness and aspect ratio of the fibers, which facilitate efficient transfer of the load from the softer PA12 matrix to the stronger fibers. 2) The presence of rigid micro-particles (BC and CNT), which stiffen the polymer matrix itself, fill the spaces between fibers, and create a rougher interface. This improves fiber-matrix adhesion and reduces the formation of micro-voids, ultimately leading to the observed increases in strength and modulus.

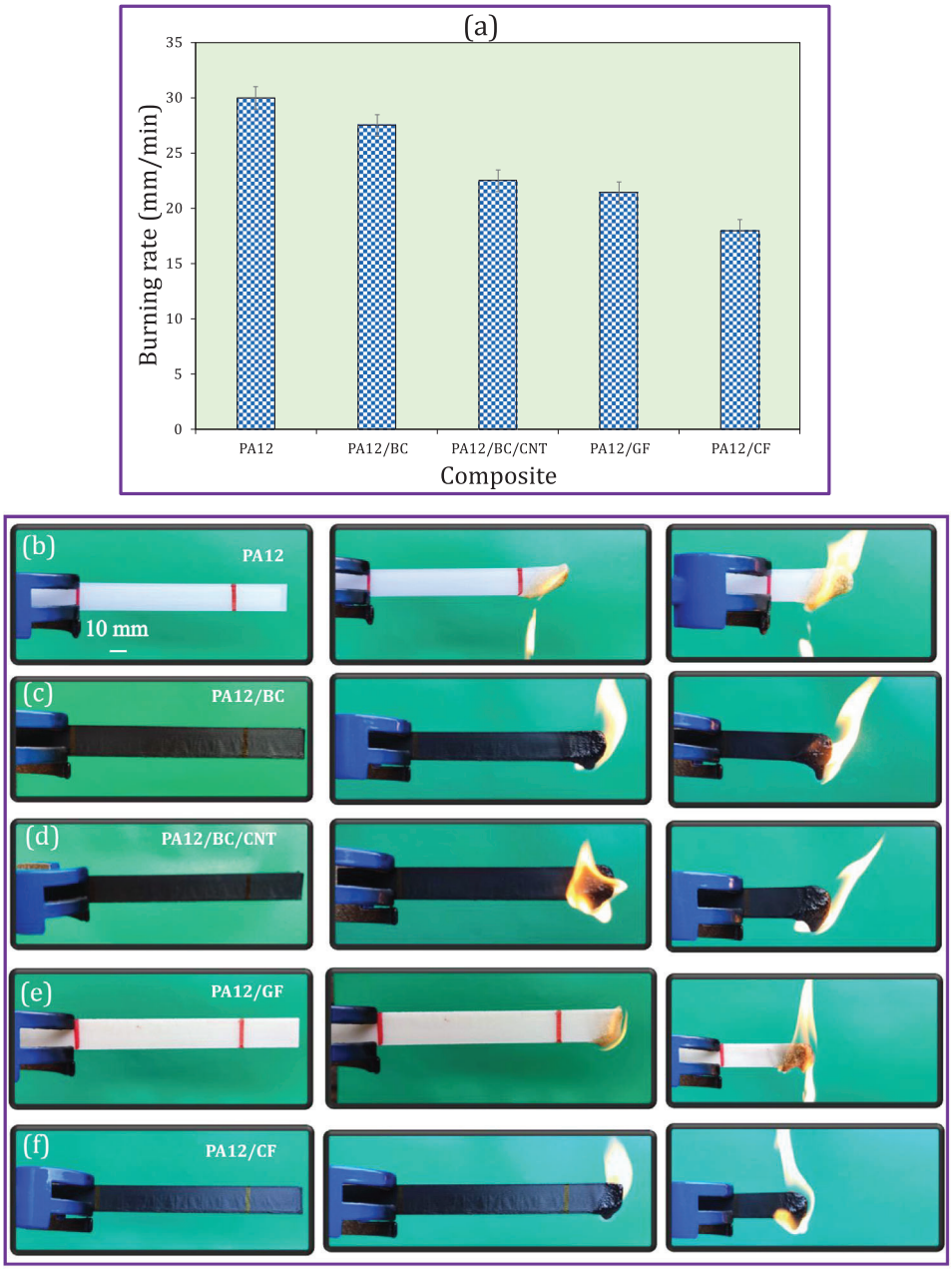

FIGURE 10 | (a) Burning rates of PA12-based composites, (b–f) PA12 and its composites before testing, during combustion, and after burning.

4.6.2 | Tensile Properties at Different Temperatures

The extensive use of polymers across industries necessitates a thorough understanding of their performance under thermal loads, as their mechanical properties are highly sensitive to temperature. A critical application is in the automotive sector, where components such as seals and connectors are subjected to fluctuating temperatures. These conditions demand contradictory material behaviors: low-temperature flexibility and impact resistance to prevent brittle fracture, and high-temperature dimensional stability and thermal resistance to inhibit deformation. Characterizing this dual thermal response is therefore fundamental to ensuring the reliability and functionality of polymers in service.

This section details the high-temperature tensile performance of the composites, examining the factors that govern their mechanical behavior. Elevated temperatures critically challenge polymers, typically reducing their stiffness and increasing flexibility. Figure 12 presents the tensile properties of PA12 and its composites tested at 50°C and 90°C. As shown in Figure 12a,b, rising temperature has a significant influence on the tensile performance of all PA12-based composites. As expected, the ultimate tensile stress decreases with increasing temperature; however, the extent of reduction varies among the different reinforcements. The primary reason for this is enhanced molecular motion above the material's T_g. This increased chain mobility allows the polymer to deform more easily, thereby lowering the stress required for elongation. Consequently, the failure strain

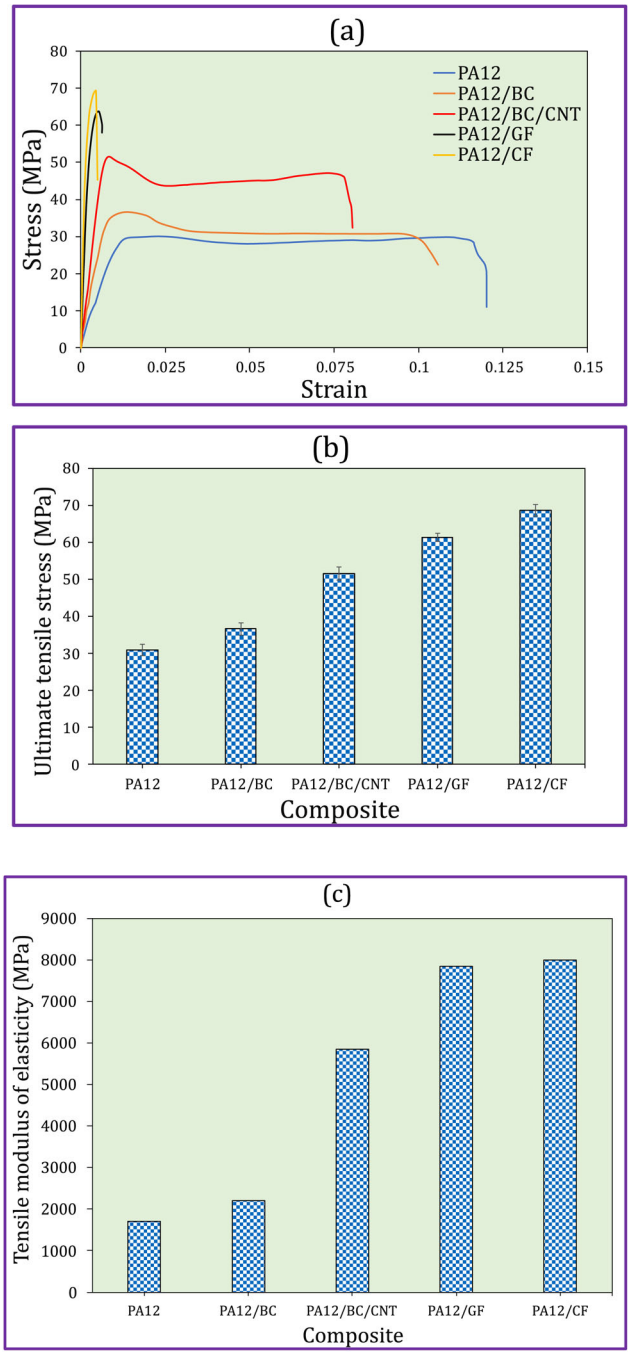

FIGURE 11 | (a) Stress-strain curves of PA12 and PA12 composites, (b, c) UTS and tensile modulus of elasticity of PA12 and PA12 composites.

generally increases due to this plasticizing effect. However, in the PA12/CF composite, this increase in ductility is limited by the constraining presence of the carbon fibers. Ultimately, the general softening of the polymer matrix leads to a pronounced reduction in strength and modulus. At 50°C (Figure 12a), PA12 demonstrated the lowest tensile strength and modulus, consistent with its inherent ductility. The incorporation of BC and BC/CNT reinforcements provided a moderate to great improvement in these properties, attributable to the stiffening effect of the particles and enhanced load transfer at the particle-matrix interface. Significantly greater enhancements were achieved with GF and CF fibers, which leveraged their high inherent stiffness and load-bearing capacity to deliver the highest performance. Notably, the BC/CNT hybrid reinforcement produced a composite with a tensile strength that was not only superior to PA12 and PA12/BC but also competitive with the fiber-reinforced composites. At 90°C (Figure 12b), the tensile strength of all materials is reduced due to thermal softening. Nevertheless, the PA12/BC/CNT composite maintains its mechanical performance more effectively than PA12 and PA12/BC, retaining approximately 28–29 MPa. Although PA12/GF and PA12/CF still show higher absolute strengths, the relative decrease in PA12/BC/CNT is smaller, indicating better thermal stability. These trends are corroborated by the UTS and modulus data in Figure 12c,d. Given this behavior, in applications where operating temperatures approach 90°C, and where moderate tensile strength is acceptable, the PA12/BC/CNT composite can serve as a potential substitute for fiber-reinforced composites, especially in cases where lower weight, improved processability, or cost reduction are desired. The presence of BC and CNT appears to enhance load transfer and thermal resistance, leading to improved performance compared to unreinforcedPA12.

Figure 13 compares the tensile stress-strain curves for the composites tested at 23, 50, and 90°C, illustrating their temperature-dependent mechanical behavior. As quantified in Figures 13a,b, both the UTS and tensile modulus exhibit a steady decline with increasing temperature for all materials. The UTS data (Figure 13a) show that PA12 drops from 30.9 MPa at 23°C to 23.5 MPa at 90°C. While BC-reinforced PA12 follows a similar trend (36.6 to 25.9 MPa), the BC/CNT composite demonstrates a less severe reduction, falling from 51.5 to 28.2 MPa. The PA12/GF and PA12/CF composites, which start with the highest strengths (63.1 and 68.6 MPa, respectively), retain the highest values at 90°C (34.2 and 31.7 MPa). These results confirm that CF and GF are the primary contributors to strength retention, while the BC/CNT combination provides significant stiffness. Figure 13b,c illustrates the variation of the tensile modulus of elasticity for PA12 and its reinforced composites as a function of temperature. A clear decreasing trend is observed for all materials, indicating that thermal softening significantly reduces stiffness as temperature increases. However, the rate of this reduction strongly depends on the type of reinforcement. At lower temperatures (near 23°C), the fiber-reinforced samples (PA12/CF and PA12/GF) exhibit the highest modulus values, exceeding 7800–8000 MPa, due to the superior stiffness of carbon and glass fibers. The PA12/BC/CNT composite shows an intermediate modulus, significantly higher than PA12 and PA12/BC, highlighting the synergistic stiffening effect of BC cellulose and CNT. As the temperature increases toward 90°C, all materials experience a substantial decrease in modulus; however, the extent of the reduction differs. PA12 and PA12/BC exhibit the steepest decline, reaching values below ~1500 MPa at 90°C. PA12/BC/CNT displays a more moderate reduction, maintaining a modulus in the range of ~3000–3500 MPa at 90°C. PA12/GF and PA12/CF retain the highest stiffness throughout the temperature range, though they also show a noticeable reduction at elevated temperatures. The fitted equations (power-law or polynomial models) show a high degree of correlation ($R^2 \approx 0.99–1$) confirming that the modulus-temperature relationship is predictable and follows consistent degradation patterns. In general, the results indicate that the PA12/BC/CNT composite maintains substantially higher

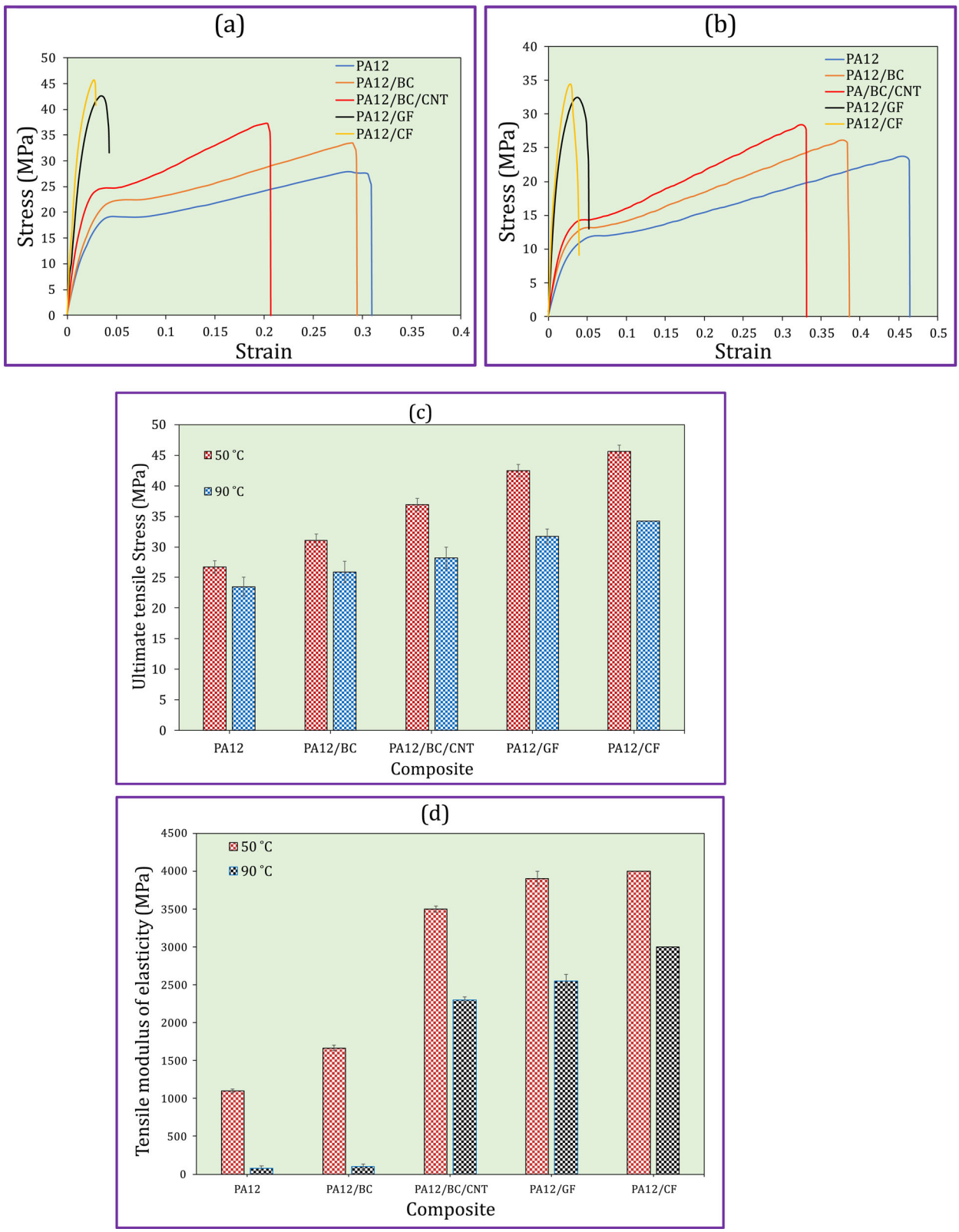

FIGURE 12 | (a, b) stress-strain curves of PA12 and PA12 composites at 50°C and 90°C, (c, d) UTS and tensile elasticity modulus of PA12 and PA12 composites.

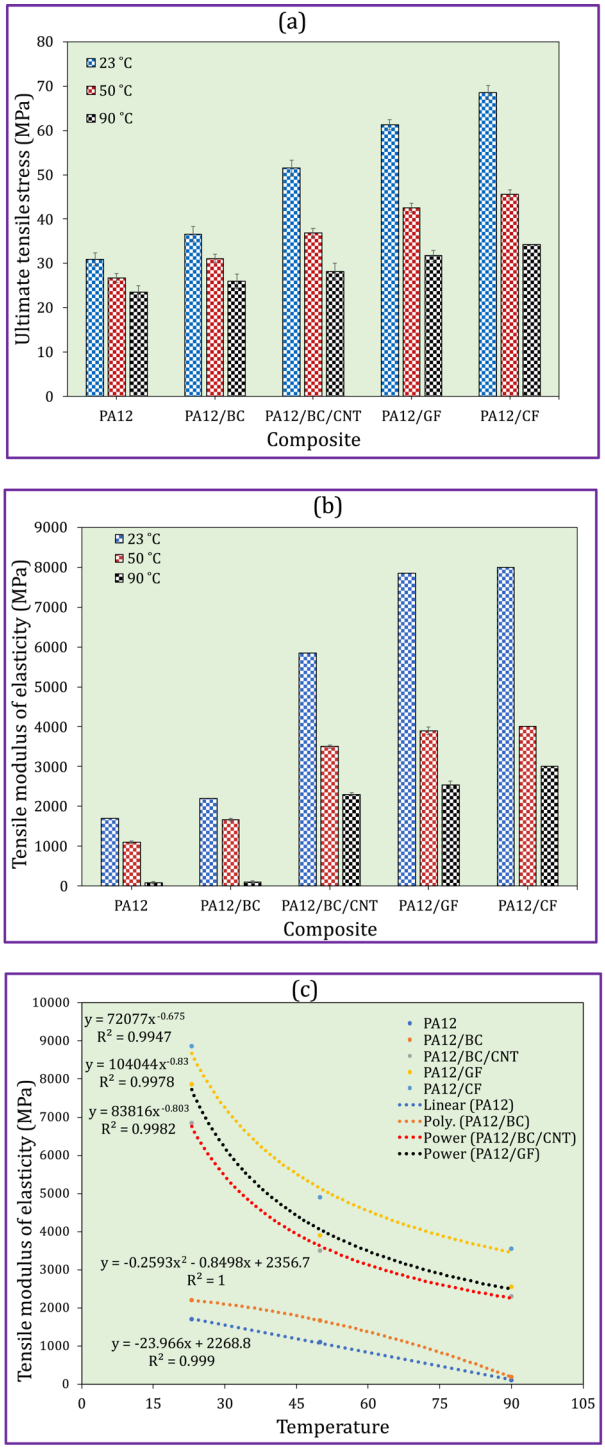

FIGURE 13 | (a, b) UTS and tensile modulus of elasticity of PA12 and PA12 composites at 23°C, 50°C, and 90°C, (C) tensile modulus of elasticity at various temperatures.

modulus at elevated temperatures compared to PA12 and PA12/BC, suggesting improved thermal stability due to the reinforcing effect of BC and CNT. Although still lower than fiber-reinforced systems, PA12/BC/CNT demonstrates a stiffness level that may be suitable for applications requiring moderate mechanical performance under thermal load. The small error bars (±1 SD) confirm the high consistency and repeatability of these measurements.

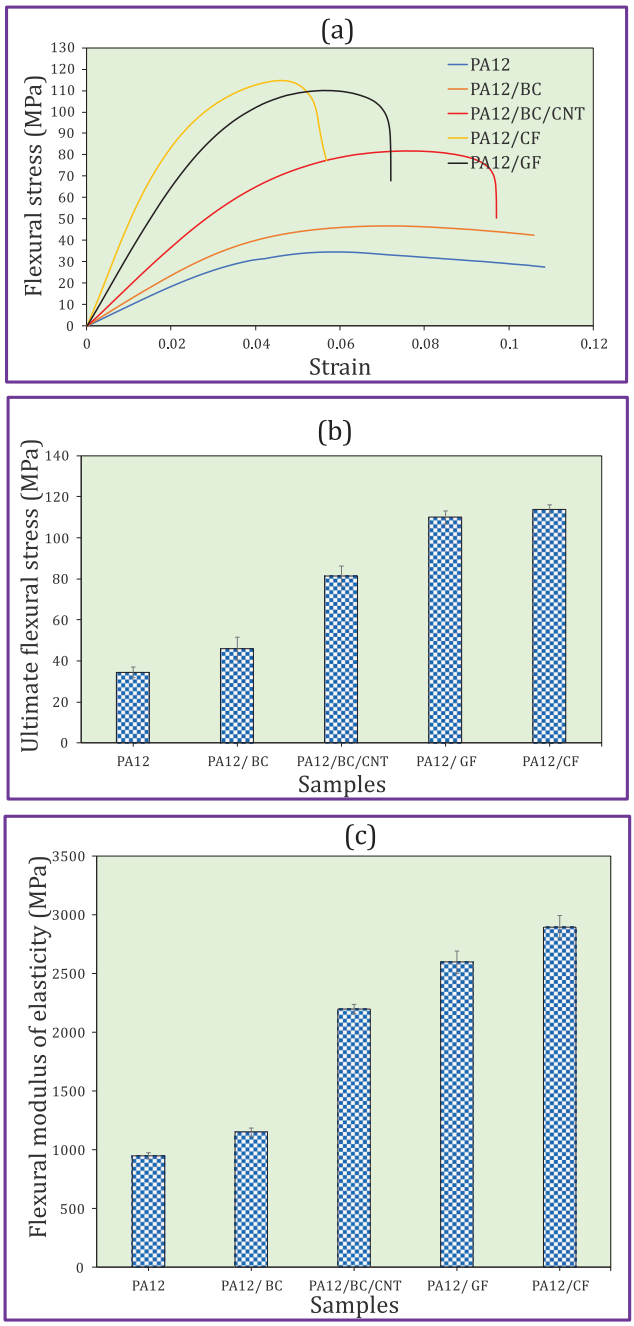

FIGURE 14 | (a) Stress–strain curves for PA12 and PA12 composites, (b, c) UTS and tensile modulus of elasticity for PA12 and PA12 composites.

4.6.3 | Flexural Test Results

The three-point bending stress-strain curves for the composites tested are illustrated in Figure 14a. As quantified in Figure 14b,c, the improvements are substantial. PA12 has a maximum flexural stress of 34.3 MPa and a modulus of 0.95 GPa. The addition of BC increases these values to 46 MPa and 1.150 GPa, respectively. A more significant jump is seen with the BC/CNT composite, which reaches 81.5 MPa and 2.2 GPa. The best performance comes from the fiber-reinforced composites, with PA12/GF and PA12/CF achieving peak stresses of 110 and 114 MPa, and moduli of 2.6 and 2.9 GPa, respectively.

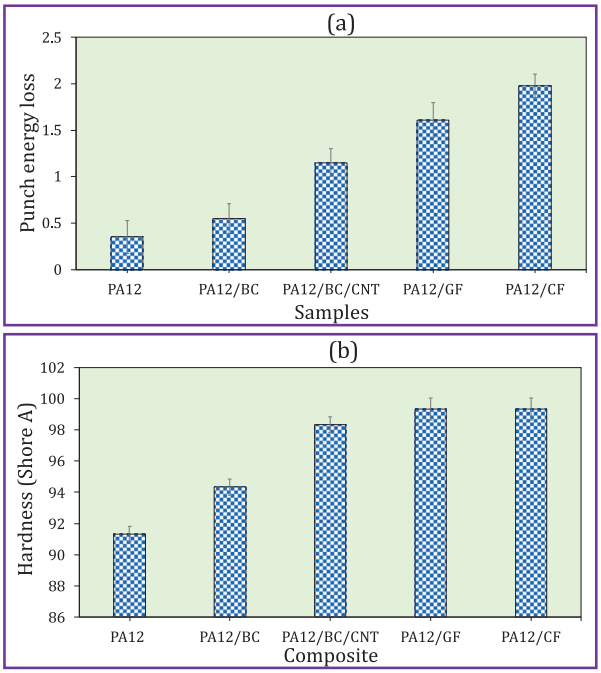

FIGURE 15 | (a) The impact energy-loss test results (b) the Shore A hardness test results for PA12 composites.

These trends align closely with the tensile test results, confirming the roles of different reinforcements. Notably, the PA12/CF composite exhibited the most dramatic improvement in flexural properties, with its maximum stress and modulus increasing by approximately 232% and 205%, respectively, compared to PA12. But in addition to fibers, the combination of BC and CNT has also been able to provide high strength.

4.6.4 | Impact Strength and Micro-Hardness Properties

In demanding industrial sectors like the automotive industry, components such as bumpers and interior panels require high impact resistance to withstand events ranging from minor debris strikes to major collisions. The punch-energy-loss test, which measures a material's capacity to absorb energy without fracturing, was used to evaluate this property.

As shown in Figure 15a, the impact resistance increased significantly with the addition of reinforcements [29]. PA12 dissipated 0.35 kJ/m^2. This value is nearly 1.5 times with the addition of BC (0.551 kJ/m^2) and more than tripled with the BC/CNT combination (1.15 kJ/m^2). The fibers-reinforced composites demonstrated the highest energy absorption, with PA12/CF reaching 1.98 kJ/m^2, a result of the fibbers' effectiveness and strong interfacial bonding with the matrix. Simultaneously, microhardness tests (Figure 15b) shows modest but consistent improvements. PA12 registered a Shore-A hardness of 91, which increased to 98 with BC/CNT, 99 with GF, and close to 100 with CF. The fact that significant gains in impact energy were achieved alongside these small increases in hardness indicates that the reinforcements enhance stiffness without inducing brittleness. The PA12/CF composite demonstrated the best performance, with its impact resistance and microhardness increasing by 465% and 8%, respectively, compared to PA12. This enhancement is attributed to mechanisms like crack deflection and bridging that allow the composite to absorb more energy before failure. The results confirm that PA12 composites reinforced with BC and CNT offer a promising combination of stiffness and impact absorption, making them suitable for manufacturing durable and safe automotive parts.

To provide a comprehensive comparison of the fabricated samples, the measured properties are presented in Figure 16 as a radar (spider) chart, including mechanical performance, impact resistance, hardness, shape-memory capability, and flammability across all material compositions. The results show that fiber-reinforced PA12, particularly PA12/CF and PA12/GF, exhibits significantly enhanced mechanical properties such as tensile strength and modulus. In contrast, PA12/BC/CNT demonstrates a more balanced performance by maintaining relatively high mechanical properties while preserving better shape recovery behavior. PA12 shows superior shape recovery but lower mechanical performance. Moreover, the PA12/BC/CNT composite demonstrates a well-balanced and superior performance profile. It shows significantly improved tensile strength at all temperatures (23°C, 50°C, and 90°C) compared to PA12 and PA12/BC. Although PA12/GF and PA12/CF reach higher absolute tensile values, the PA12/BC/CNT composite maintains its performance more consistently across the entire temperature range. This behavior indicates enhanced thermal stability and improved retention of mechanical properties at elevated temperatures. Taken together, these results highlight PA12/BC/CNT as a competitive alternative to fiber-reinforced PA12, offering a combination of mechanical performance, flame retardancy, and shape-memory functionality that is difficult to achieve with conventional fiber-reinforced systems in advanced AM and 4D-printing contexts.

5 | Composite base PA12 Structures

Recent advances in multi-material composite 3D printing have enabled the fabrication of high-performance components that combine the intrinsic properties of constituent materials with the advantages of architected geometries [30]. Cellular lattice metamaterials, such as honeycomb and auxetic structures, offer high specific strength and stiffness together with excellent energy absorption efficiency [31, 32]. When combined with materials capable of dissipating energy, such geometries enable lightweight structures suitable for impact mitigation applications, including automotive crash zones, bumper systems, energy-absorbing components, and robotic and sporting equipment. In addition, lightweight architected designs contribute to reduced material usage and environmental impact within a circular economy framework [33]. In this study, a novel 3D-printable multifunctional composite system was extended from material development to structural implementation through QZS mechanical metamaterials. Auxetic, honeycomb, and honeycomb–circle hybrid meta-composite structures (Figure 17) were fabricated via 3D printing using PA12, PA12/BC/CNT, PA12/GF, and PA12/CF.

The mechanical performance of the meta-structures was evaluated under loading-unloading cycles at a constant crosshead speed of 5 mm/min. Specimens with an initial height of 40 mm were compressed to 25% strain for auxetic structures and 50% strain for honeycomb and honeycomb-circle hybrid structures.

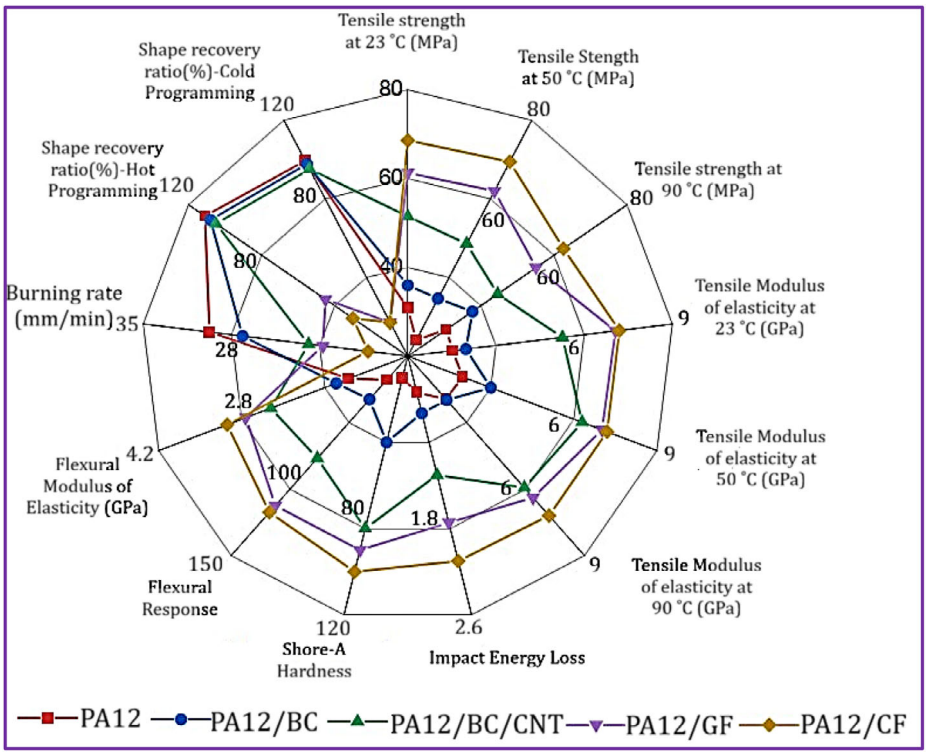

FIGURE 16 | Spider chart summarizing and presenting a consolidated comparison of the experimentally measured properties of PA12 and its composites.

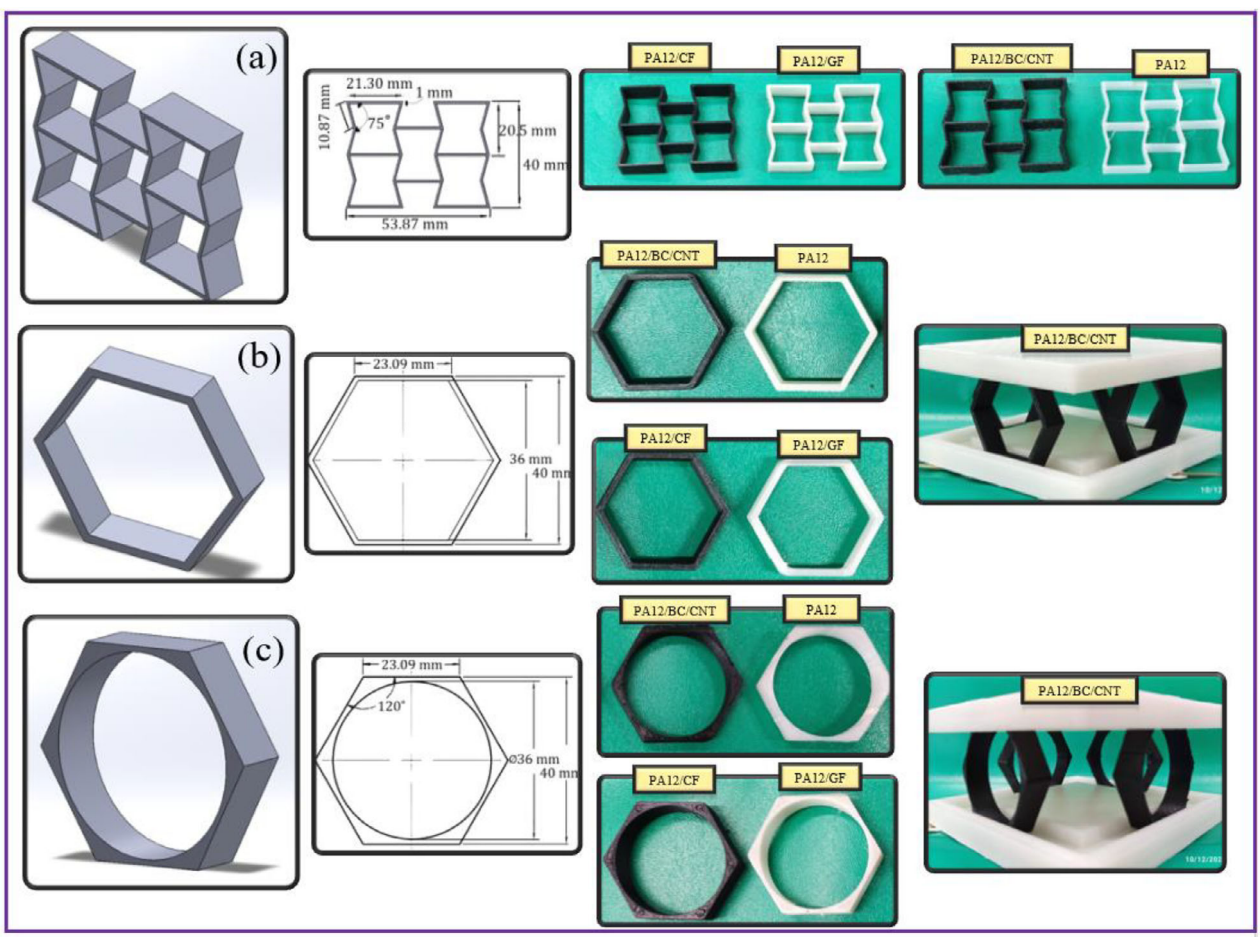

FIGURE 17 | Designed and 3D printed structure meta-composites, (a) auxetic, (b) honeycomb, (c) honeycomb-circle hybrid.

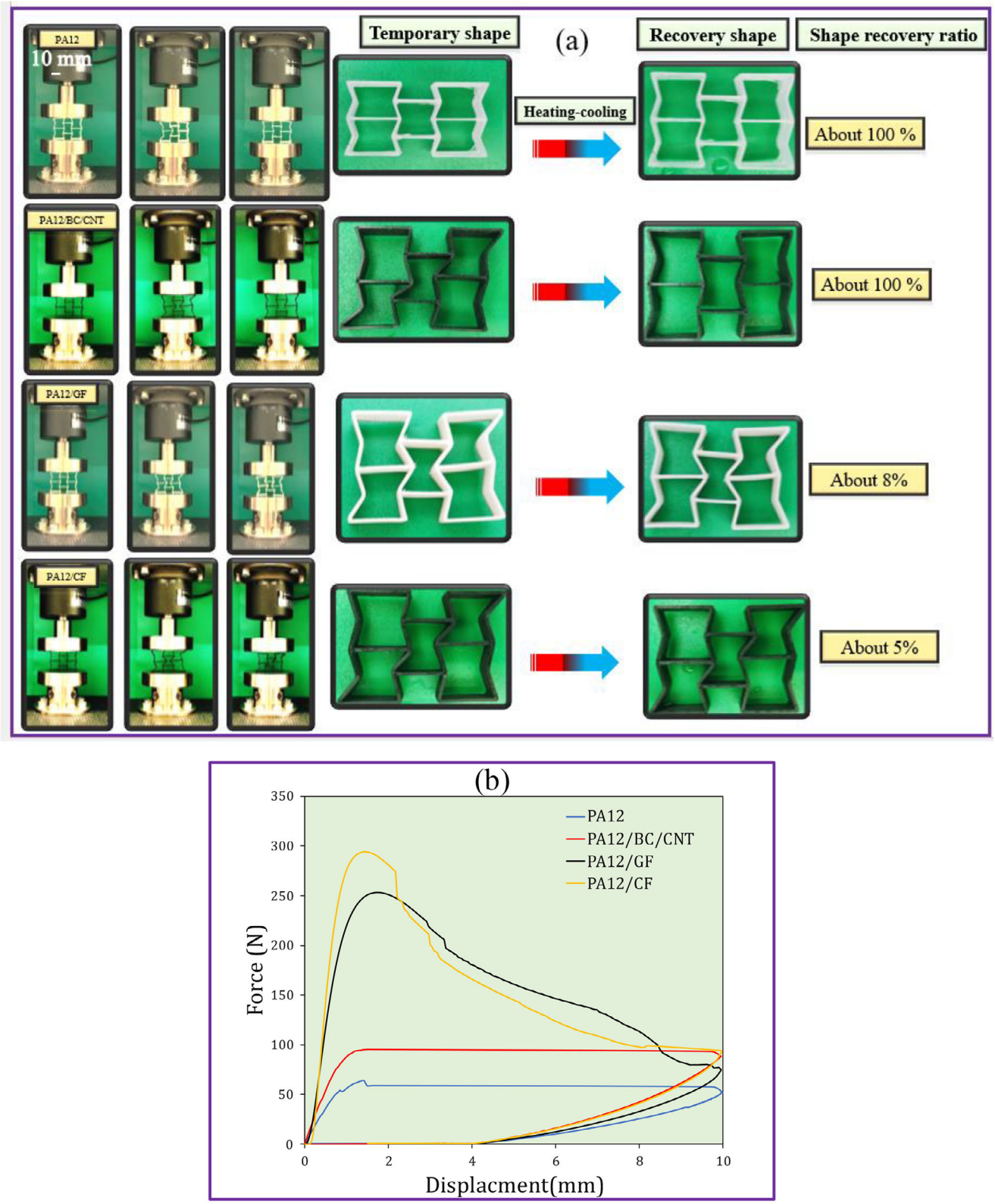

FIGURE 18 | The force-displacement response of various meta-composites under a loading-unloading-recovery cycle of PA12 and its composites under 25% and 50% compression (a, b), auxetic (c, d), honeycomb (d, e), honeycomb-circle hybrid.

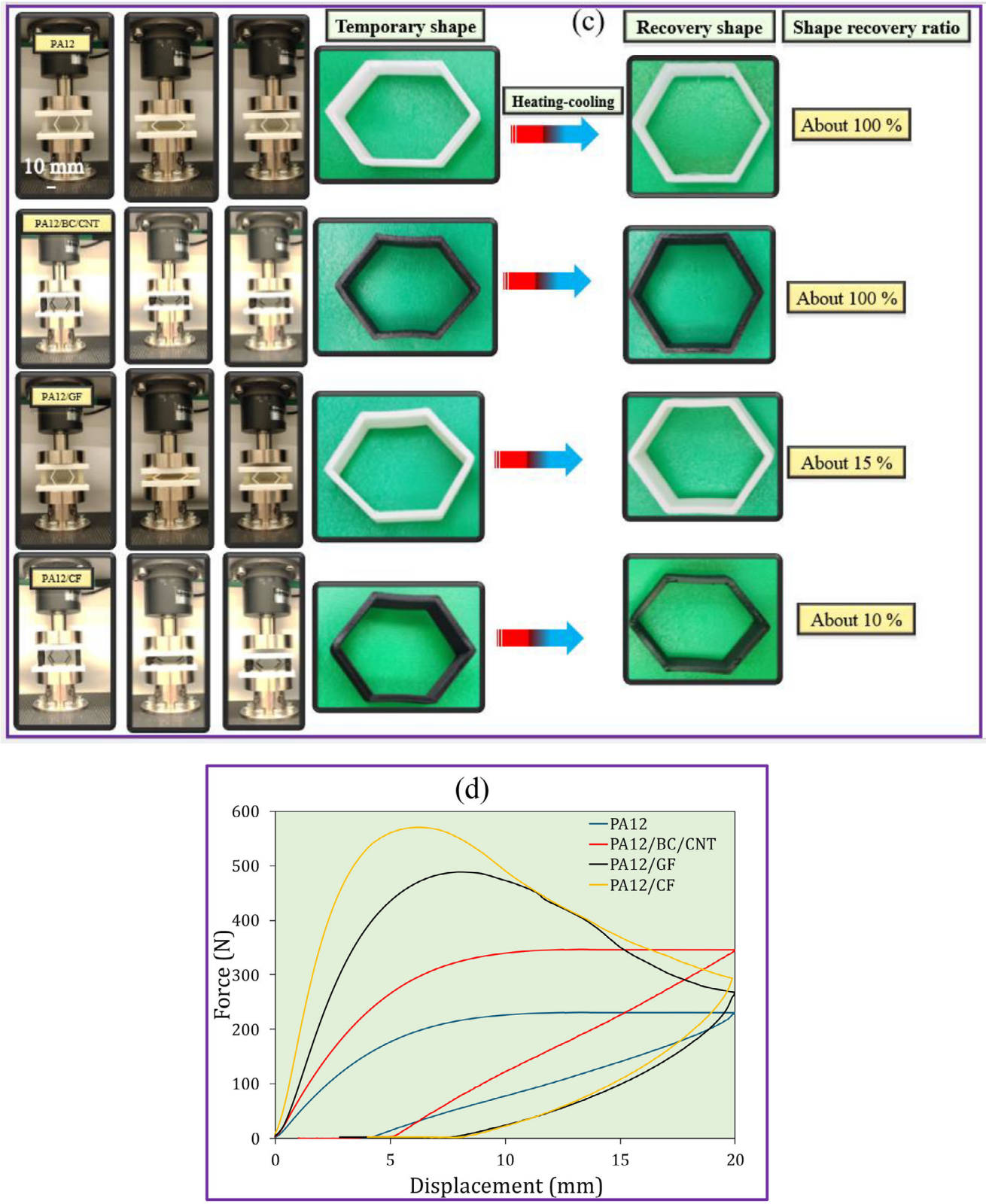

FIGURE 18 | (Continued)

The deformation states and shape recovery behavior are presented in Figure 18. PA12 and PA12/BC/CNT meta-structures fully recovered their original shapes upon heating above the glass transition temperature, achieving shape recovery ratios of approximately 100% after unloading from both compression levels. In contrast, PA12/GF and PA12/CF meta-composites exhibited permanent inelastic deformation and limited recovery (≈5%–15%), indicating a loss of structural stability due to the absence of effective shape-memory behavior. This permanent set is attributed to inelastic matrix deformation and micro- to macro-scale

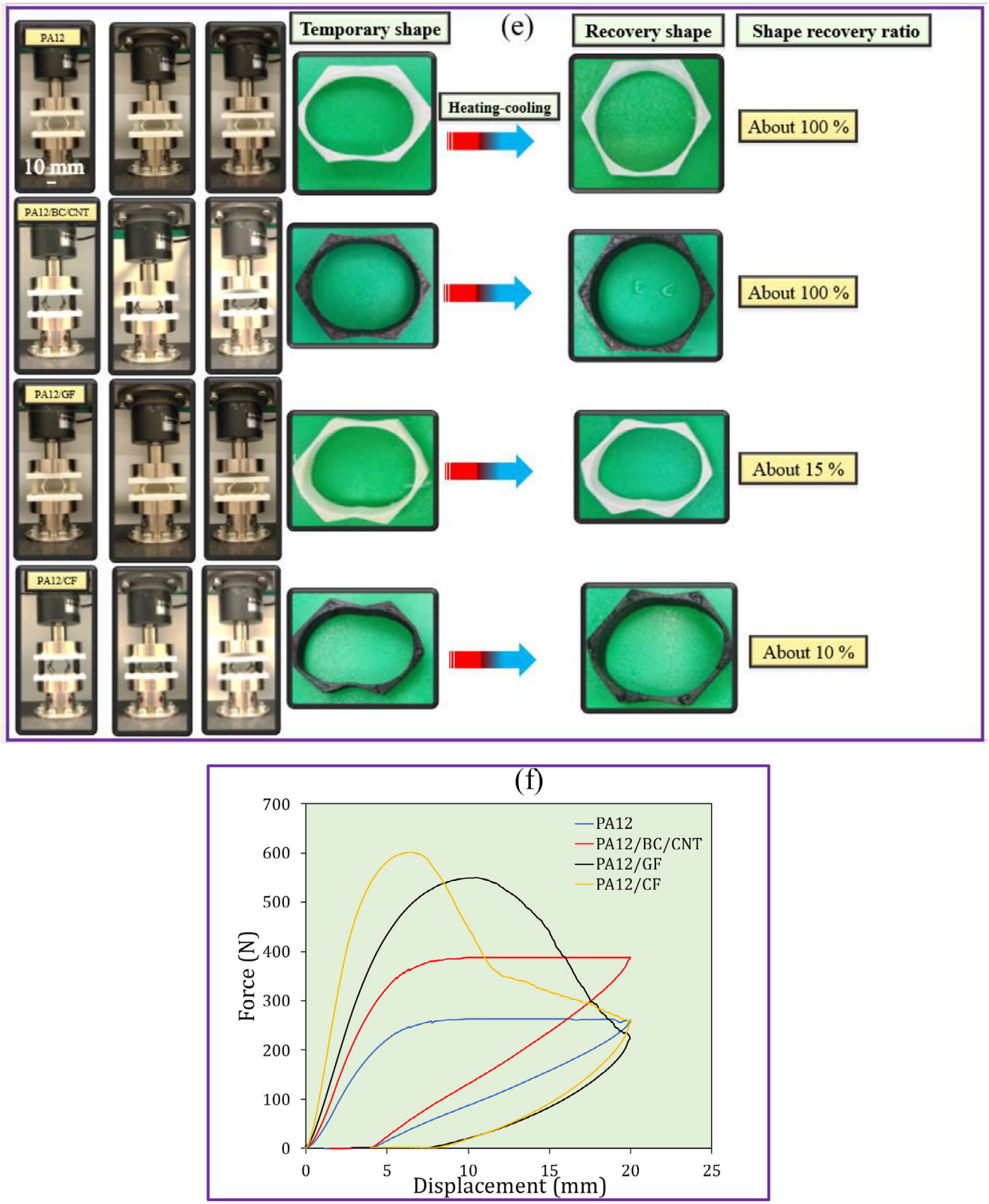

FIGURE 18 | (Continued)

damage in the fiber–matrix system. The corresponding force-displacement responses are also shown in Figure 18, revealing distinct stiffness characteristics among the meta-composites. PA12 and PA12/BC/CNT meta-structures exhibited force-regulating behavior with a pronounced reduction in stiffness over a defined displacement range, indicative of QZS-like response. In contrast, the PA12/GF and PA12/CF meta-composites displayed negative stiffness behavior, in which the reaction force decreased with increasing displacement. As summarized in Figure 19a, incorporation of BC/CNT resulted in higher stiffness and increased

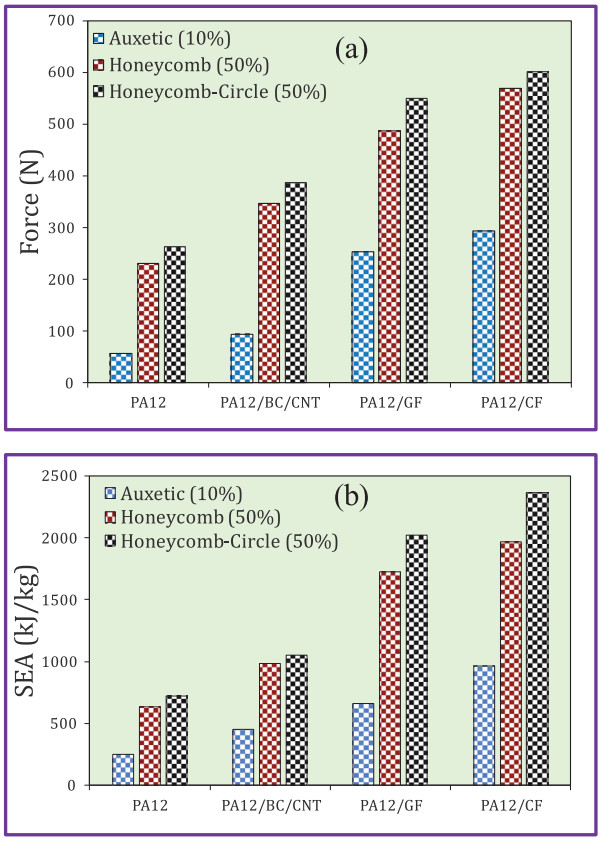

FIGURE 19 | (a) Maximum force and (b) SEA values within 25% and 50% compression for 3D-printed meta structures.

maximum reaction forces compared with PA12, while maintaining a more stable force response than CF-GF-reinforced systems. Furthermore, honeycomb-circle hybrid structures consistently outperformed conventional honeycomb designs due to increased corner thickness and improved stress redistribution enabled by the circular features.

Energy absorption and dissipation were evaluated during loading-unloading cycles using force-displacement hysteresis loops. The absorbed energy corresponds to the area under the loading curve, while the dissipated energy is represented by the enclosed hysteresis loop area; the recoverable energy is associated with the area under the unloading curve. Energy dissipation arises from Visco-elastic and Hyper-elastic behavior, plastic deformation, and buckling-type instabilities. In this study, the specific energy absorption (SEA) of the meta-composites was quantified from the experimentally obtained force-displacement curves and normalized by specimen mass, as presented in Figure 19b. PA12 exhibited the lowest SEA value (720.5 kJ/kg for the honeycomb-circle hybrid), reflecting limited energy absorption dominated by matrix yielding. Incorporation of reinforcements significantly enhanced the energy absorption capacity. In particular, the PA12/BC/CNT meta-composite achieved an SEA of 1054.2 kJ/kg, corresponding to an improvement of approximately 46% compared to PA12. The fiber-reinforced systems exhibited the highest SEA values, with PA12/CF reaching 2366.0 kJ/kg, more than three times that of PA12.

6 | Future Perspectives and Potential Applications

The present findings support the development of a comprehensive database of PA12-based composites for advanced functional applications. Compared with degradable polymers such as PLA, PA12 is non-degradable and maintains stable performance over a wide temperature range. The developed composites combine high thermo-mechanical strength, effective impact energy dissipation, mechanical compliance, and a QZS metamaterial architecture that enables controlled load response. In addition, the material system demonstrates improved flame retardancy and moisture resistance and, through the use of renewable resources such as bamboo charcoal, offers potential benefits in terms of sustainability and end-of-life considerations. These synergistic attributes make the proposed metamaterial suitable for a wide range of applications, including automotive, sporting, and robotic systems. The tuneable mechanical response of the QZS architecture further enhances structural resilience and efficiency, particularly in applications involving combined thermal and impact loading. Acting as both an energy absorber and an overload limiter, the QZS design effectively reduces peak impact forces. Beyond the structural advantages, PA12 reinforced with BC and CNT provides additional functional benefits. Reduced wettability and moisture uptake make the material suitable for prolonged use in warm or humid environments, while enhanced flame-retardant behavior provides an additional layer of thermal safety. Collectively, these properties result in a mechanically robust, thermally resilient, and flame-retardant metamaterial, supporting its suitability for diverse real-world applications. Representative conceptual designs illustrating potential application domains are shown in Figure 20. The developed hybrid composites demonstrate strong potential for advanced lightweight structures. Future work will focus on optimizing the BC/CNT hybrid ratios, integrating the composites into multi-material FFF printing, and exploring electrically triggered shape memory through CNT conductive networks. These developments may facilitate potential applications in lightweight automotive and robotic systems.

7 | Conclusion

This study developed and systematically evaluated multifunctional PA12-based composites tailored for fused filament fabrication and 4D-printing applications. By incorporating BC, CNT, GF, and CF, the work establishes a comprehensive comparison between natural, hybrid, and conventional reinforcement strategies in terms of mechanical, thermal, functional, and flame-retardant performance. Among the investigated systems, the PA12/BC/CNT composite demonstrated a uniquely balanced performance profile. Unlike GF- and CF-reinforced composites, which provided high stiffness and strength at the expense of shape-memory capability, the BC/CNT hybrid simultaneously enhanced stiffness, strength, thermal stability, flame retardancy, hydrophobicity, and shape-memory behavior. SEM analysis confirmed uniform dispersion and strong interfacial bonding of BC and CNT within the PA12 matrix, supporting efficient load transfer and energy dissipation mechanisms. Thermomechanical analysis showed that BC/CNT reinforcement improved resistance to thermal softening and enabled better retention of

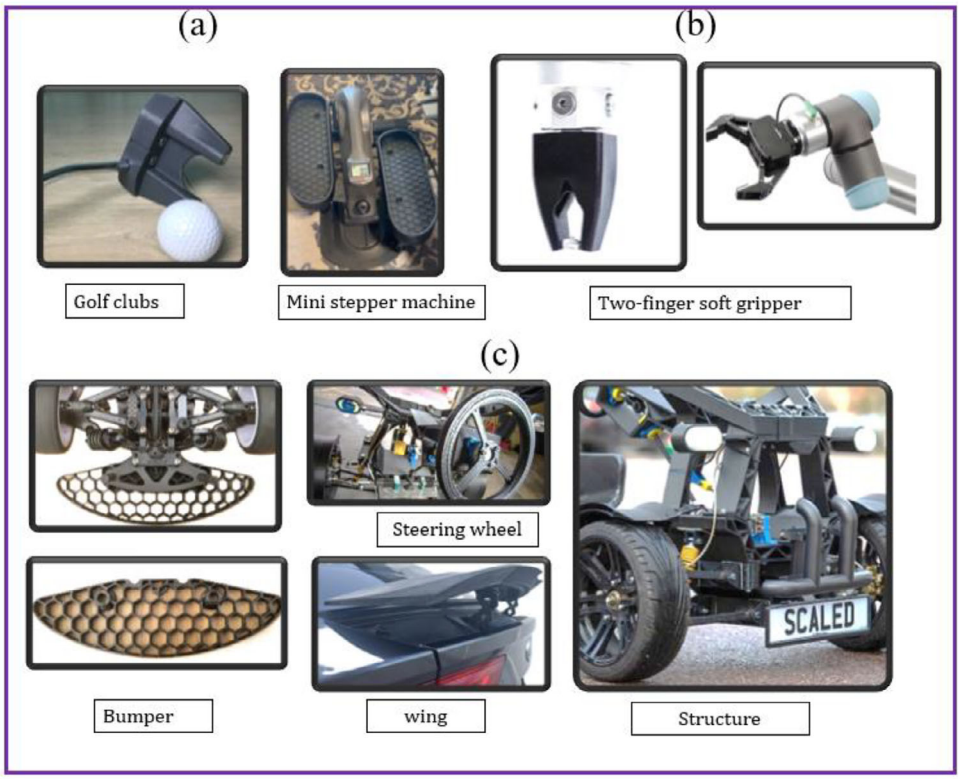

FIGURE 20 | Illustration of potential application domains for the proposed composite for a wide range of applications, including sport (a), robotics (b), and automotive (c).

mechanical properties at elevated temperatures compared with PA12. Flammability testing further demonstrated that BC/CNT significantly reduced burning rates and suppressed dripping, achieving fire retardancy comparable to fiber-reinforced systems while maintaining material compliance. Mechanical testing confirmed that although GF and CF provided the highest absolute stiffness and strength, the PA12/BC/CNT composite offered a favorable compromise between mechanical performance and functional behavior, including impact resistance and shape-memory recovery. Extending from material development to structural implementation, architected meta-composites fabricated from PA12/BC/CNT exhibited excellent shape recovery and force-regulating behavior under compression, enabling high specific energy absorption and quasi-zero-stiffness-like response. These features are not achievable with conventional fiber-reinforced systems and highlight the potential of hybrid-based reinforcements for advanced mechanical metamaterials.

In summary, the PA12/BC/CNT composite emerges as a promising, sustainable, and multifunctional alternative to traditional fiber-reinforced PA12 for lightweight structural components, energy-absorbing systems, and deployable 4D-printed architectures. While developed primarily for FFF, these materials also show potential for conventional processing routes such as injection molding, supporting broader industrial adoption.

Acknowledgements

This work was supported by the Engineering and Physical Sciences Research Council (EPSRC) [award no: EP/Y011457/1], the EPSRC's Innovation Launchpad Network+ RiR scheme [grant no: EP/W037009/1, EP/X528493/1; award no: RIR26C230615-6], and the Research Program by Seoul National University of Science and Technology [grant no: 2025-1318].

Conflicts of Interest

The authors declare no conflict of interest.

Data Availability Statement

The data that support the findings of this study are available from the corresponding author upon reasonable request.

References

1. S. Qi, X. Gao, Y. Su, Y. Zhou, X. Dong, and D. Wang, "Effect of Carbon Nanotubes on Mechanical Properties of Polyamide 12 Parts by Fused Filament Fabrication," *Polymer* 247 (2022): 124784, https://doi.org/10.1016/j.polymer.2022.124784.

2. N. Vidakis, M. Petousis, E. Velidakis, et al., "Multi-functional Polyamide 12 (PA12)/Multiwall Carbon Nanotube 3D Printed Nanocomposites With Enhanced Mechanical and Electrical Properties," *Advanced Composite Materials* 31 (2022): 630–654, https://doi.org/10.1080/09243046.2022.2076019.

3. M. Bodaghi, K. Rahmani, M. L. Dezaki, C. Branfoot, and J. Baxendale, "3D/4D printed Bio-composites Reinforced by Bamboo Charcoal and Continuous Flax Fibres for Superior Mechanical Strength, Flame Retardancy and Recoverability," *Polymer Testing* 143 (2025): 108709, https://doi.org/10.1016/j.polymertesting.2025.108709.

4. M. Y. Khalid, A. Otabil, O. S. Mamoun, K. Askar, and M. Bodaghi, "Transformative 4D Printed SMPs into Soft Electronics and Adaptive Structures: Innovations and Practical Insights," *Advanced Materials Technologies* 10 (2025): 00309.

5. A. N. Dickson, H. M. Abourayana, and D. P. Dowling, "3D Printing of Fibre-Reinforced Thermoplastic Composites Using Fused Filament Fabrication—A Review," *Polymers* 12 (2020): 2188, https://doi.org/10.3390/polym12102188.

6. B. Brenken, E. Barocio, A. Favaloro, V. Kunc, and R. B. Pipes, "Fused Filament Fabrication of Fiber-Reinforced Polymers: A Review," *Additive Manufacturing* 21 (2018): 1–16, https://doi.org/10.1016/j.addma.2018.01.002.

7. M. Feldmann and A. K. Bledzki, "Bio-based Polyamides Reinforced With Cellulosic fibers—Processing and Properties," *Composites Science and Technology* 100 (2014): 113–120, https://doi.org/10.1016/j.compscitech.2014.06.008.

8. S. Krishna, I. Sreedhar, and C. M. Patel, "Molecular Dynamics Simulation of Polyamide-based Materials—A Review," *Computational Materials Science* 200 (2021): 110853, https://doi.org/10.1016/j.commatsci.2021.110853.

9. W. Griehl and D. Ruestem, "Nylon-12-preparation, Properties, and Applications," *Industrial & Engineering Chemistry* 62 (1970): 16–22, https://doi.org/10.1021/ie50723a005.

10. A. Dorigato, M. Brugnara, and A. Pegoretti, "Novel Polyamide 12 Based Nanocomposites for Industrial Applications," *Journal of Polymer Research* 24 (2017): 96, https://doi.org/10.1007/s10965-017-1257-9.

11. M. Kurokawa, Y. Uchiyama, T. Iwai, and S. Nagai, "Performance of Plastic Gear Made of Carbon fiber Reinforced Polyamide 12," *Wear* 254 (2003): 468–473, https://doi.org/10.1016/S0043-1648(03)00020-6.

12. B. Ucpinar Durmaz, E. Artykbaeva, and A. Aytac, "Fabrication and Performance of Short Glass fiber Reinforced Polyamide Composites," *International Journal of Polymer Analysis and Characterization* 29 (2024): 589–601, https://doi.org/10.1080/1023666X.2024.2394222.

13. S. Jindal, F. Manzoor, N. Haslam, and E. Mancuso, "3D printed Composite Materials for Craniofacial Implants: Current Concepts, Challenges and Future Directions," *The International Journal of Advanced Manufacturing Technology* 112 (2021): 635–653, https://doi.org/10.1007/s00170-020-06397-1.

14. A. Doğru, M. Ö. Seydibeyoğlu, and C. Ayranci, "The Effect of Interface Enhancement on the Mechanical Properties of Fibre-reinforced PA6 Matrix Composites in Material Extrusion-based Additive Manufacturing," *Progress in Additive Manufacturing* 10 (2025): 361–374.

15. M. Petousis, N. Vidakis, N. Mountakis, V. Papadakis, and L. Tzounis, "Three-Dimensional Printed Polyamide 12 (PA12) and Polylactic Acid (PLA) Alumina (Al_2O_3) Nanocomposites With Significantly Enhanced Tensile, Flexural, and Impact Properties12 (PA12) and Polylactic Acid (PLA) Alumina (Al_2O_3) Nanocomposites With Significantly Enhanced Tensile, Flexural, and Impact Properties," *Nanomaterials* 12 (2022): 4292, https://doi.org/10.3390/nano12234292.

16. T. Czigány and J. Karger-Kocsis, "A Comparison of the Mechanical Behaviour of Weft-Knitted Glass and Carbon Fiber Fabric-Reinforced Polyamide-12 Composites Produced With Commingled Staple Yarns," *Polymers and Polymer Composites* 9 (2001): 491–498, https://doi.org/10.1177/096739110100900801.

17. K. Rahmani, H. Malekmohammadi, A. Haque, et al., "Bio-composite Design and 3D Printing of Soft Multi-functional Meta-structures With Tuneable Quasi-constant Force," *Applied Materials Today* 47 (2025): 102961, https://doi.org/10.1016/j.apmt.2025.102961.

18. M. N. Ahmad, M. R. Ishak, M. Mohammad Taha, F. Mustapha, and Z. Leman, "A Review of Natural Fiber-Based Filaments for 3d Printing: Filament Fabrication and Characterization," *Materials* 16 (2023): 4052.

19. K. Rahmani, C. Branfoot, and M. Bodaghi, "Bio-derived PA11/Bamboo Charcoal/Glass Fiber Composites for Fused Filament Fabrication, Warpage Control, Strength and Flame Retardancy," *Virtual and Physical Prototyping* 20 (2025): 2589848, https://doi.org/10.1080/17452759.2025.2589848.

20. M. Sabet, "Advancements in Halogen-free Polymers: Exploring Flame Retardancy, Mechanical Properties, Sustainability, and Applications," *Polymer-Plastics Technology and Materials* 63 (2024): 1794–1818, https://doi.org/10.1080/25740881.2024.2359633.

21. B. W. Liu, H. B. Zhao, and Y. Z. Wang, "Advanced Flame-Retardant Methods for Polymeric Materials," *Advanced Materials* 34 (2022): 2107905, https://doi.org/10.1002/adma.202107905.

22. K. Rahmani, C. Branfoot, S. Karmel, K. Lindsey, and M. Bodaghi, "Flexible Bio-composites With Continuous Natural Fibre and Bamboo Charcoal: Enhanced Flame Retardancy, Mechanical Resilience, Energy-absorbing & Printability Performance," *Virtual and Physical Prototyping* 20 (2025): 2534845, https://doi.org/10.1080/17452759.2025.2534845.

23. J. Wang, Z. Wang, Z. Song, L. Ren, Q. Liu, and L. Ren, "Programming Multistage Shape Memory and Variable Recovery Force With 4D Printing Parameters," *Advanced Materials Technologies* 4 (2019): 1900535, https://doi.org/10.1002/admt.201900535.

24. H. Doostmohammadi, M. Baniassadi, M. Bodaghi, and M. Baghani, "4D Printing of Magneto-Thermo-Responsive PLA/PMMA/Fe_3 O_4 Nanocomposites With Superior Shape Memory and Remote Actuation," *Macromolecular Materials and Engineering* 309 (2024): 2400090, https://doi.org/10.1002/mame.202400090.

25. S. S. Kumar, J. S. Akmal, and M. Salmi, "4D printing of Shape Memory Polymer with Continuous Carbon Fiber," *Progress in Additive Manufacturing* 9 (2024): 1985–1995, https://doi.org/10.1007/s40964-023-00553-1.

26. K. Rahmani, S. Ravanbod, M. L. Dezaki, C. Branfoot, and M. Bodaghi, "Pellet-fed Continuous-silk-fibre 3D/4D Printing of PLA/Bamboo-charcoal Bio-composites With Shape Recovery and Thermomechanical Stability," *Materials & Design* 264 (2026): 115704, https://doi.org/10.1016/j.matdes.2026.115704.

27. M. Lalegani Dezaki, C. Branfoot, J. Baxendale, and M. Bodaghi, "Bio-Based Gradient Composites for 3D/4D Printing With Enhanced Mechanical, Shape Memory, and Flame-Retardant Properties," *Macromolecular Materials and Engineering* 310 (2025): 2400276, https://doi.org/10.1002/mame.202400276.

28. E. Paari-Molnar, W. N. A. F. Qa'dan, K. Kardos, et al., "Biomedical Applications of 3D-Printed Polyamide: A Systematic Review," *Macromolecular Materials and Engineering* 310 (2025): 00156.

29. D. Maher, M. Piekarczyk, B. Rezaei, and A.-I. Bunea, "Beyond 3D: Smart Material Systems for Microscale 4D Printing," *Advanced Materials Technologies* 10 (2025): 2401950.

30. I. M. Alarifi, "Revolutionising Fabrication Advances and Applications of 3D Printing With Composite Materials: A Review," *Virtual and Physical Prototyping* 19 (2024): 2390504, https://doi.org/10.1080/17452759.2024.2390504.

31. J. Ma, H. Zhang, T.-U. Lee, H. Lu, Y. M. Xie, and N. S. Ha, "Auxetic Behavior and Energy Absorption Characteristics of a Lattice Structure Inspired by Deep-sea Sponge," *Composite Structures* 354 (2025): 118835, https://doi.org/10.1016/j.compstruct.2024.118835.

32. M. Shadman, H. Ahmadi, D. Rahmatabadi, and M. Seidi, "Study on the Shape Memory Performance of 4D-Printed Auxetic Cellular Structures With Energy Absorption Application," *Macromolecular Materials and Engineering* 311 (2025): 00320, https://doi.org/10.1002/mame.20250032.

33. C. Zeng, L. Liu, W. Bian, and Y. Liu, "4D printed Electro-Induced Continuous Carbon Fiber Reinforced Shape Memory Polymer Composites With Excellent Bending Resistance," *Composites Part B: Engineering* 194 (2020): 108034, https://doi.org/10.1016/j.compositesb.2020.108034.

Supporting Information

Additional supporting information can be found online in the Supporting Information section.

Supporting File: mame70212-sup-0001-SuppMat.docx.